UNIVERSITY OF CALIFORNIA
SANTA CRUZ

GENETIC DETERMINANTS of ANTIMICROBIAL PEPTIDE RESPONSES in *Vibrio cholerae*

A dissertation submitted in partial satisfaction
of the requirements for the degree of

DOCTOR OF PHILOSOPHY
in

MICROBIOLOGY AND ENVIRONMENTAL TOXICOLOGY

by

LIZETT J GONZALEZ CARREON

August 2026

The Dissertation of Lizett J Gonzalez Carreon is approved:

_____
Professor Fitnat Yildiz, Chair

_____
Professor Karen Ottemann

_____
Professor Michael Patnode

_____
Professor Seth Rubin

_____
Donald Smith
Vice Provost and Dean of Graduate Studies

Table of Contents

List of Tables

List of Figures

Abstract

Genetic Determinants of Antimicrobial Peptide Responses

in *Vibrio cholerae*

By Lizett J Gonzalez Carreon

Cationic antimicrobial peptides (CAMPs) are key components of innate immunity that provide defense against bacterial pathogens. *Vibrio cholerae*, the causative agent of cholera, colonizes the small intestine, where it encounters CAMPs produced by the host epithelium. Although several CAMP-responsive pathways have been characterized, the full complement of genetic determinants that enable *V. cholerae* to sense, adapt to, and survive CAMP stress remains incompletely understood. Bacterial responses to environmental stress often involve two-component signaling (TCS) systems, including the CarRS system, which is critical for CAMP resistance and is one of the few regulators known to negatively regulate biofilm formation in *V. cholerae*. However, the mechanisms underlying CarRS-mediated antimicrobial resistance and biofilm regulation remain poorly understood. To comprehensively define the genetic and regulatory mechanisms underlying the *V. cholerae* CAMP response, we combined whole-genome expression profiling with genome-wide random-barcode transposon-site sequencing (RB-Tn-seq). We challenged transposon libraries with subinhibitory concentrations of polymyxin B to identify genes required for fitness during CAMP stress. This approach identified known CAMP resistance determinants, including *carRS*, *almEFG*, and *lpxN*, as well as previously unreported genes involved in lipopolysaccharide core and O-antigen biosynthesis, outer membrane biogenesis, and envelope homeostasis. To further investigate CarRS, we examined the phosphorylation states of CarS and CarR to determine their influence on antimicrobial resistance and biofilm formation. These findings show that CarRS phosphorylation partially influences both phenotypic outcomes, linking this TCS activity to CAMP resistance and biofilm maintenance. Together, these findings expand the genetic framework of the *V. cholerae* CAMP stress

response and provide new insight into how envelope homeostasis and CarRS signaling coordinate antimicrobial resistance and biofilm regulation.

Acknowledgments

I begin by thanking Dr. Fitnat Yildiz for her support throughout my Ph.D. Dr. Yildiz has guided me to become a diligent scientist and, through her dedicated time, helped me complete milestones during unprecedented times- from grad student strikes and the pandemic to California wildfires. I will be forever thankful for her commitment to improving my development in experimental design and purpose. She would bring in-depth analysis to our conversations during our meetings. She has given me the push I needed to believe in myself during difficult times and has been an example not only as a scientist, but as a mentor and leader. I will hold our conversations, group meetings, and lab outings close to my heart. As I move to my next stage as a scientist and professional, I have learned so much from you; in particular, anything is possible with the right set of controls and attitude: “let’s go for it.” Thank you.

I want to give a special thank you to my thesis committee, Dr. Karen Ottemmann, Dr. Michael Patnode, and Dr. Seth Rubin. I had the opportunity to share my research progress and ideas with an excellent team of experts, all of whom were also on my qualifying exam committee. It has been an honor to have your feedback guide me throughout my time at UCSC. You all saw my potential from my qualifying exam through annual committee meetings, when I shared my results. I felt supported, but above all, I felt the comfort of knowing I was making progress and that I could communicate my results, which was a crucial moment for me and increased my confidence.

As I reflect, none of this would be possible without the relentless support of past and current Yildiz lab members. Dr. Jennifer Teschler, Dr. Carmen Schwechheimer, and Dr. Avatar Joshi were my first mentors as a rotation student and new lab member. Dr. Jin-Hwan Park helped

me with cloning and presentation preparation and always offered incredible knowledge and his time. I want to thank Dr. Bao Nguyen, who helped me with so many mundane tasks and shared food ideas and recommendations. Thank you to Dr. Giordan Kitts for your curiosity about new lab techniques and your bioinformatics expertise, which greatly contributed to my project. I would like to give a special thank you to Dr. Anna Potapova, with whom I had the privilege of working in the same bay. Thank you for your help, from teaching me how to run beautiful western blots to teaching protocols with an emphasis on teaching skills. Together, we made our bay a welcoming place for our undergrads.

I would like to thank my community at UCSC: Dr. Juliana Nzongo and Dr. Nick Santigago for your friendship through my Ph.D. Thank you to Dr. Amanda Carbajal, Dr. Cristobal Morfin, Dr. Raymond Lopez-Magaña, Dr. Anny Mogollon, Dr. Roxanna Villalobos, and Dr. Michelle Gomez Parra for all your friendship, support, and words of encouragement. Thank you to soon-to-be doctors Anthony Rodriguez, Brian Rivera, Cristian Vargas, Melissa Estrada, Ana Ponce, and Eric Huang.

I would like to thank my number one support system. My sounding board and comedic relief, my loving boyfriend Jeremy Dodsworth. You have listened to many of my experiences at UCSC and in Santa Cruz. Through the highs and lows, you have always assured me things would be okay.

I would like to dedicate my thesis work and efforts to my mother, Carmela Carreon DeGonzalez, and my brother, Addison Isaac Gonzalez Carreon. None of this would have been possible, or even exist, if my mother had not decided to bring us to the United States. My mother made the life-changing decision to move to a country that did not want her here and expected less-than treatment. My brother, the eldest, taught me how to handle complicated situations, work hard with my hands, and carry myself in rooms where I am the

only person of color. Together, we fought and worked hard; we supported one another, shared difficulties and accomplishments. I am forever grateful for those teachings and experiences; thank you, Mom and brother.

Chapter 1 Introduction

Microorganisms live in changing environments and face a wide variety of physical, chemical, and biological stimuli that drive adaptation and evolution. These include variations in nutrient availability, oxygen, pH, temperature, osmolarity, and antibiotic exposure (1). Facultative human pathogens must also adapt to host-generated factors, including bile, antimicrobial peptides, immune defenses, and interactions with the microbiota. For bacteria that alternate between environmental and host-associated lifestyles, understanding how they receive, respond to, and integrate these diverse signals is particularly important (2).

Bacteria have evolved signal transduction networks that enable them to sense and respond to diverse signals. For example, two-component signal transduction systems (TCSs), composed of a sensor histidine kinase and a response regulator, detect environmental stimuli and regulate gene expression to promote cellular responses necessary for detection (3, 4), response, and adaptation(5–7). Responses and adaptation to environmental signals include membrane remodeling, metabolic changes, and transitions between motile and biofilm lifestyles (8).

Biofilm formation enhances *Vibrio cholerae* survival and infectivity in the environment. Biofilms are aggregates of microbial cells encased in an extracellular matrix, beginning with a bacterial cell that swims toward the surface using its polar flagella and establishes cell-to-surface interactions through mannose-sensitive hemagglutinin pili (9, 10). These cells then grow, divide, and secrete extracellular matrix components, including exopolysaccharide (EPS) specific to Vibrio (VPS) and matrix proteins (1, 11, 12). In response to environmental and metabolic signals, biofilm cells disperse and can restart biofilm formation in a more favorable environment (13). The CarRS TCS negatively regulates biofilm gene expression,

and in strains lacking *carRS*, biofilm formation increases compared with the wild type (14). However, the mechanism behind this regulation is not fully understood.

The overall objective of this work is to identify genetic determinants involved in the CAMP response and to determine how they interact with pathways that regulate biofilm formation.

Chapter 2 Genetic determinants of cationic antimicrobial peptide response in *Vibrio cholerae*

2.1 **Abstract**

Cationic antimicrobial peptides (CAMPs) are key components of innate immunity and provide defense against bacterial pathogens. *Vibrio cholera*e, the causative agent of cholera, colonizes the small intestine (15) where it encounters CAMPs produced by the epithelium. Although some studies have described CAMP-responsive pathways, the full complement of genes whose products sense and adapt to CAMPs in *V. cholerae* remains unknown. To comprehensively map the genetic determinants of *V. cholerae* CAMP sensing, regulation, and protective responses, we performed whole-genome expression profiling and genome-wide random-barcode transposon-site sequencing (RB-Tn-seq) analyses. *V. cholerae* transposon libraries were challenged with subinhibitory concentrations of the cationic antimicrobial peptide (CAMP) polymyxin B to identify genes that contribute to bacterial fitness during CAMP stress. The screen identified a broad set of genes whose disruption reduced fitness in the presence of polymyxin, including known systems such as the two-component signal transduction system *carRS*; the *almEFG* genes, which are involved in lipid A modification with glycine and diglycine; and *lpxN*, a lipid A secondary hydroxy-acyltransferase. Our work also identified a set of genes whose association with the polymyxin B response had not previously been reported in *V. cholerae*. These include genes required for lipopolysaccharide core and O-antigen biosynthesis; genes involved in outer membrane biogenesis; VC1039, VC2156, and VC0851; and uncharacterized genes in *V. cholerae,* VCA0802, VCA0714, and VC1500. To validate these findings, we generated deletion mutants of selected genes and assessed the fitness of the resulting strains under challenge with polymyxin B, LL-37, and envelope stress conditions. These studies confirmed the roles of multiple cell envelope homeostasis and modification systems in the polymyxin B response. These findings identify additional components of *V. cholerae*'s CAMP response network and broaden the molecular framework for understanding the pathogen's survival.

2.2 **Introduction**

During infection, pathogenic microorganisms experience various environmental stresses. One such stress is exposure to antimicrobial peptides (APs), which are polypeptides of fewer than 100 amino acids synthesized by the host (1, 2). Two major classes of antimicrobial peptides, the defensins and cathelicidins, are produced by immune and epithelial cells. Defensins (α and β types) are cationic peptides with specific structural properties, produced by neutrophils, epithelial cells, and Paneth cells in the intestine (1, 2). Cathelicidins, including LL-37, are a structurally distinct family of peptides primarily found in neutrophil granules (1, 2). Both classes of peptides kill bacteria by disrupting bacterial membranes via electrostatic interactions (2, 3). Polymyxins are antibiotics produced by various strains of the bacterium *Paenibacillus polymyxa* and act similarly: they disrupt bacterial membranes via electrostatic interactions (4). Cationic antimicrobial peptides (CAMPs) typically interact with the outer membrane of Gram-negative bacteria by binding to the lipid A moiety of lipopolysaccharide (LPS). CAMP binding displaces the divalent cations Mg^{2+} and Ca^{2+}, which generally stabilize adjacent LPS molecules, thereby weakening the outer membrane. This disturbance enhances membrane permeability and, at higher doses, causes membrane damage, cell lysis, and loss of cellular contents. Bacteria use several defense methods to overcome these effects. These include outer membrane remodeling, lipid A alteration, efflux pump activation, outer membrane vesicle formation, and altered expression of outer membrane proteins (5–10).

Vibrio cholerae, the pathogen responsible for the disease cholera, encounters CAMPs during intestinal colonization and has developed a multi-layered network of CAMP resistance mechanisms (16). The primary resistance mechanism modifies the lipid A domain of LPS with glycine and diglycine residues via the AlmEFG pathway, reducing the net negative charge of the outer membrane (11). A second lipid A modification process is mediated by a phosphoethanolamine transferase, ethanolamine transferase A (*eptA*), which transfers the

amino-residue phosphoethanolamine (pEtN) to lipid A, conferring CAMP resistance at acidic pH when the AlmEFG pathway is downregulated (12). Efflux pumps also mediate CAMP resistance by pumping these compounds out of the cell. In *V. cholerae*, the Resistance-Nodulation-Cell-Division (RND) efflux pump VexAB-TolC represents the efflux component of CAMP resistance (13). The biofilm growth state confers additional CAMP protection, in which outer membrane vesicles (OMVs) containing the biofilm matrix protein Bap1 facilitate CAMP sequestration away from the cell surface (14). CAMP response also includes an extra cytoplasmic stress response, which is controlled by the alternate sigma factor RpoE. OmpU, an outer membrane protein, regulates RpoE activation and thereby contributes to CAMP resistance (15). Furthermore, the virulence regulator ToxR modulates CAMP resistance by regulating *ompU* transcription (16). *V. cholerae* employs a second regulatory system, the two-component regulatory system CarRS, that regulates CAMP resistance by directly activating transcription of the *almEFG* operon (17, 18*)*. The *carRS* genes are found in an operon with *ompV*, which encodes an outer membrane protein predicted to sense polymyxin and activate CarRS-mediated CAMP resistance mechanisms (19). Despite significant progress in characterizing individual CAMP resistance determinants in *V. cholerae*, no comprehensive genome-wide mutational analysis has been performed to determine the CAMP resistance landscape. *V. cholerae* encounters CAMPs in the small intestine, which provides evidence that CAMPs are important defense mechanisms for the mammalian host (17).

In this study, we used a multi-omics approach to identify genetic determinants of the CAMP response in *V. cholerae*. Pathogens frequently encounter CAMPs at sub-inhibitory concentrations (20). Thus, we first assessed the response to sub-MIC polymyxin B via RNA-seq and, as a complementary approach, conducted an unbiased, genome-wide screen to identify genes contributing to fitness differences using Barseq. We identified the known determinants of polymyxin B response discussed above, along with VC1039, VC0851, VC2156, VCA0802, VCA0714, and VC1500, which contribute to polymyxin B resistance.

Furthermore, these genes also confer resistance to CAMP LL-37. None of these genes were involved in the general envelope stress response, as they did not show sensitivity when grown in the presence of membrane-disturbing agents, bile, and SDS-EDTA.

2.3 **Results**

2.3.1. Genes differentially regulated in response to sub-inhibitory polymyxin B levels.

To identify genes and regulatory networks activated in response to sub-inhibitory concentrations of polymyxin B in *V. cholerae*. We used a sub-inhibitory concentration of polymyxin B equal to ½ the minimum inhibitory concentration (MIC). This concentration was used to assess cell response at a non-lethal level, where wild-type growth is affected but not impaired. We compared global transcript levels in wild-type *V. cholerae* cells exposed to polymyxin B versus cells not exposed to polymyxin B. We did this by growing overnight cultures, subculturing cells to an O.D. of 0.5, and exposing them to ½ MIC of polymyxin B. We identified genes that were up- or down-regulated upon polymyxin B exposure. Thresholds were $| \log_2 (\text{fold-change}) | < 1$ (indicating a lower transcript level) and log2 (fold-change)> 1 (indicating a higher transcript level) for cells grown in the presence of polymyxin B compared to LB, with an adjusted p-value < 0.05. A total of 227 genes were differentially expressed (Figure 2A); of these, 209 genes were significantly upregulated (Table 2.1), and 13 genes were significantly downregulated in the presence of polymyxin B (Table 2.2). The 5 most significant pathways are iron acquisition, protein transport and secretion, envelope stress response, and protein folding, with a positive Normalized Enrichment Score (NES), NES is refers to the gene set enrichment analysis that identifies genes involved in a specific pathway upregulated (positive score) or downregulated (negative score) in the presence of polymyxin B compared to no polymyxin B. Pathogenesis and virulence pathways have negative NES scores (Figure 2B). The significantly upregulated genes include the CarRS TCS and

members of the CarR regulon, which have previously been identified as important for polymyxin B resistance.

Figure 2.1 Transcripts differentially expressed in the presence of polymyxin B.
A) Volcano plot of total genes found to be differentially regulated in wild-type *V. cholerae* in the presence of by 25μg/ml of polymyxin B compared to cells grown in LB. Blue dots indicate genes with decreased transcript abundance in the presence of polymyxin B, and red dots indicate genes with increased transcript abundance. Grey lines indicate cutoffs for transcript abundance: a log2 fold-change greater than 1 (vertical lines) and an adjusted p-value < 0.05 (horizontal line). A $|\log_2$ (fold-change) $|$ less than 1 indicates a lower transcript level, and a log2 (fold-change) greater than 1 indicates a higher transcript level when cells were grown in the presence of polymyxin B compared to LB. B) GSEA bubble plot displaying the 5 most significant pathways. Normalized Enrichment Score (NES): positive values indicate enrichment among upregulated genes, and negative values indicate enrichment among downregulated genes. Dot size represents the number of leading-edge genes driving the enrichment, and dot color represents -log10(adjusted p-value); lighter green indicates greater significance.

.

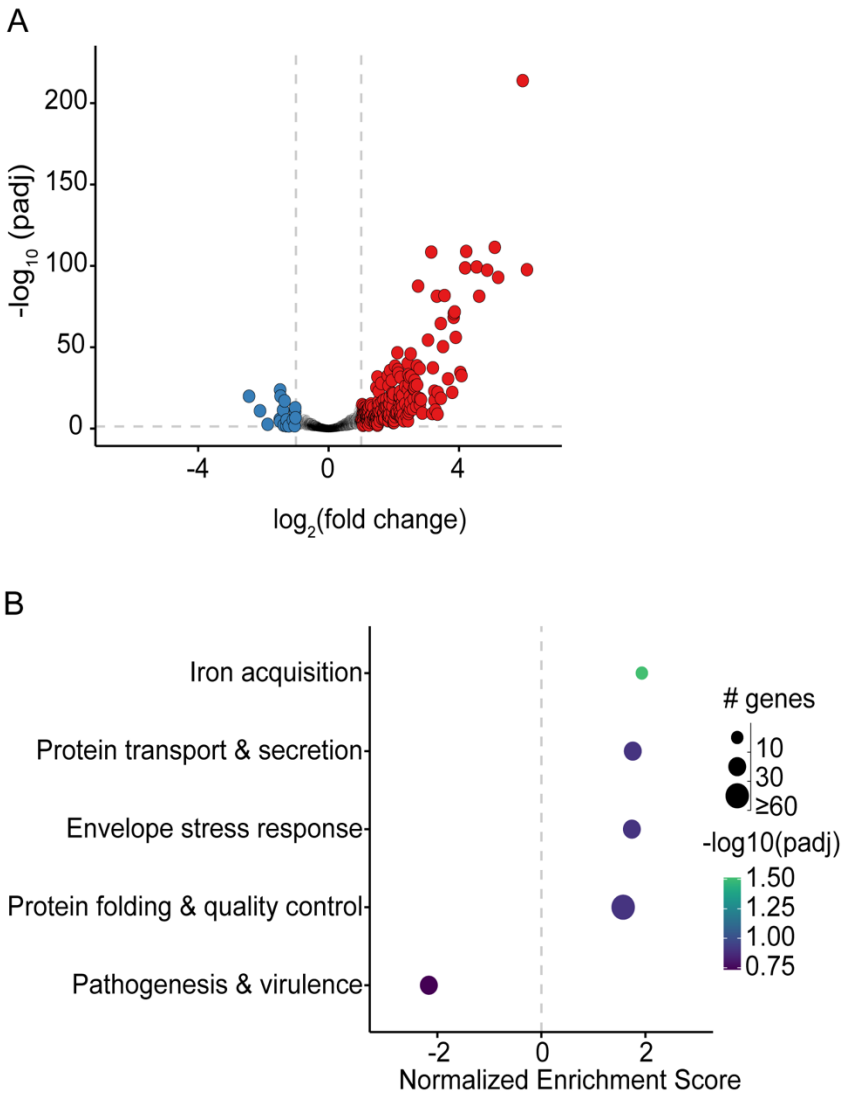
A
200
150
100
50
0
-log10 (padj)
-4
0
4
log2(fold change)
B
Iron acquisition
Protein transport & secretion
Envelope stress response
Protein folding & quality control
Pathogenesis & virulence
-2
0
2
Normalized Enrichment Score
genes
10
30
≥60
-log10(padj)
1.50
1.25
1.00
0.75

Table 2.1 Upregulated transcripts in wild-type cells grown in LB with and without polymyxin B.

Gene	Gene name	Log_2 fold change	Protein description
VC0773		6.08	Vibrio-specific isochorismate synthase
VCA0732	*sipA*	5.95	hypothetical protein
VC1573	*fumC*	5.10	Fumarate hydratase
VC0774	*vibA*	4.86	dehydrogenase
VC0772	*vibE*	4.62	2,3-dihydroxybenzoate-AMP ligase
VC2209	*vibF*	4.54	siderophore biosynthesis
VC0873		4.22	hypothetical protein
VCA0845		4.19	hypothetical protein
VC1572		4.08	hypothetical protein
VC1688		4.04	Manganese transporter
VC2694	*sodA*	3.90	Superoxide dismutase
VC2211	*viuA*	3.87	Outer membrane protein
VC1637	*dbfQ*	3.84	hypothetical protein
VC1638	*dbfR*	3.84	Response regulator
VC1563	*hlyD*	3.79	putative Secretion protein
VC1565	*tolC*	3.66	outer membrane protein
VC1566	*varD*	3.56	putative ABC-type antimicrobial peptide transport system, permease component

Gene	Gene name	Log_2 fold change	Protein description
VC1317	*virK*	3.51	putative virulence factor
VCA0976		3.44	hypothetical protein
VC1318	*ompV*	3.44	Outer membrane porin
VC0771	*VibB*	3.35	Isochorismatase
VC0775	*VibH*	3.34	Vibriobactin synthase
VC1567	*varD*	3.32	Putative ABC-type antimicrobial peptide transport system, permease component
VC0879		3.28	Ribosomal protein
VC0878		3.25	Ribosomal protein
VCA0977		3.24	Thioredoxin domain containing protein
VC1564		3.18	Hypothetical protein
VC1568	*varF*	3.15	ABC transporter, ATP-binding protein
VC1306		3.05	Putative ATPase
VCA0715		2.87	Conserved hypothetical protein
VCSEN_ancRNA609		2.83	Small regulatory RNA
VC0474	*irgB*	2.81	Transcriptional regulator
VC0776	*viuP*	2.80	ABC transporter, ferric vibriobactin-binding protein
VC1307		2.79	Conserved hypothetical
VC0566	*degP*	2.74	Protease

Gene	Gene name	Log_2 fold change	Protein description
VC0777		2.73	ABC transporter, permease protein
VC1639	*dbfS*	2.72	Sensor histidine kinase
VCA0966		2.71	Hypothetical protein
VC1224		2.69	Conserved hypothetical protein
VCA0064	*hutR*	2.66	Heme receptor
VCA0716		2.64	Putative cytochrome
VCA0231		2.62	Putative transcriptional regulator
VCA0159		2.62	Putative universal stress protein
VC1319	*carS*	2.61	Sensor histidine kinase
VCA0175		2.59	ATPase
VC0554		2.53	Zn-dependent peptidase
VC2240	*padC*	2.52	Phenolic acid decarboxylase
VC1320	*carR*	2.51	Response regulator
VCA0174		2.51	DUF58 domain-containing protein
VCA0591		2.49	Peptide transport system, periplasmic component
VC0711	*clpB*	2.49	Chaperone
VCA0909		2.48	Oxidase homolog
VCA1051		2.47	Conserved hypothetical protein

Gene	Gene name	Log_2 fold change	Protein description
VC1571		2.45	Cytochrome quinol oxidase, subunit
VCA0066		2.45	Conserved hypothetical protein
VC1570		2.44	Putative Cytochrome ubiquinol oxidase subunit
VCA0648		2.43	Conserved hypothetical protein
VCA0232		2.43	Fragment of Enterobactin receptor
VCA0065		2.43	Putative peptidase
VCA0911		2.39	Biopolymer transport protein
VC1009		2.35	Conserved hypothetical protein
VC2047		2.35	Oxidoreductase, short-chain dehydrogenase/reductase
VCA0910	*tonB*	2.31	Outer membrane protein
VCA0576		2.28	Heme receptor
VC0778		2.26	ABC transporter, permease protein
VC0091		2.26	Putative O-Methyltransferase
VCA0951		2.26	Putative heavy-metal-binding protein
VCSEN_ancRNA112		2.24	Small RNA
VC2210	*viuB*	2.22	Vibriobactin utilization protein
VCA0913		2.22	ABC-type hemin
VCA0590		2.21	Peptide ABC transporter, permease protein

Gene	Gene name	Log_2 fold change	Protein description
VCA0139		2.20	Putative Acyl-CoA synthetase
VC1577	*almG*	2.20	Glycyltransferase
VCA0912	*exbD1*	2.19	Biopolymer transport protein
VCA0915	*hmuV*	2.19	Hemin import ATP-binding protein
VC0200	*fhuA*	2.19	Ferrichrome outer membrane receptor
VC1409	*vcE*	2.18	Multiple-Drug Resistance efflux protein
VC1899		2.17	Conserved hypothetical
VC0553		2.17	Putative ABC transporter
VCA0588		2.14	ABC transporter, ATP-binding
VCA0170		2.13	Hypothetical
VCA0169		2.11	Hypothetical
VC1827		2.10	Mannose-6-phosphate isomerase
VCA0067		2.09	Conserved hypothetical
VC1578	*almF*	2.08	Glycine-carrier
VCA0914	*hmuU*	2.06	permease
VC1579	*almE*	2.04	dual aminoacyl-adenyltransferase/carrier protein ligase
VC2466	*rseA*	2.04	Sigma-E negative regulatory
VCA0721		2.01	Orphan protein

Gene	Gene name	Log_2 fold change	Protein description
VCA1093	*cheW-2*	2.01	Purine-binding chemotaxis
VC1410	*vceA*	1.99	Multiple-drug resistance Efflux protein
VC1061		1.99	Putative cysteine synthase
VCA0589		1.98	Putative ABC transporter permease
VC2485	*leuO*	1.97	HTH-type transcriptional regulator
VCA0722		1.96	Conserved hypothetical protein
VCA0171		1.96	Uncharacterized Von willebrand factor type A domain protein
VC2674	*hslU*	1.95	ATP-dependent, protease ATP-binding subunit
VC1987	*siP*	1.94	Putative starvation lipoprotein
VCA1102		1.93	putative Phosphoethanolamine transferase
VCA0172		1.89	Putative bacteroides aerotolerance operon protein
VC0779	*fepC*	1.88	Ferric enterobactin transport ATP-binding protein
VC0034	*dsbA*	1.87	Thiol-disulfide interchange protein
VCA0047		1.87	Putative Multidrug resistance efflux pump
VC0780	*vibD*	1.87	Vibriobactin synthase component
VC2675	*hslV*	1.86	ATP-dependent protease
VC2418	*dsbC*	1.85	Thiol-disulfide interchange protein

Gene	Gene name	Log_2 fold change	Protein description
VCA0168		1.84	Hypothetical protein
VC1873		1.84	Putative stress response protein
VCA1070		1.84	Conserved hypothetical protein
VC0556	*gshA*	1.81	Glutamate-cysteine ligase
VCSEN_ancRNA63		1.81	VC0353 antisense
VC2467	*rpoE*	1.79	RNA polymerase sigma-E factor
VC1902	*dsbB*	1.77	Disulfide bond formation protein
VCA0907	*hugZ*	1.77	Heme utilization protein
VC1743		1.74	Putative 1-aminocyclopropane-1-carboxylate deaminase
VCA0048		1.72	Conserved hypothetical protein
VC1401	*cheB-1*	1.71	Putative chemotaxis response regulator
VC0977		1.70	Putative thioredoxin domain-containing protein
VCA0789		1.69	Conserved hypothetical protein
VC0188	*prlC*	1.69	Oligopeptidase
VC0886		1.68	Putative Class II aldolase/adducin
VC2701	*dsbD*	1.65	Thiol-disulfide interchange protein
VC1411	*vceB*	1.64	Multiple-drug resistance efflux protein
VC1485		1.63	Conserved hypothetical protein

Gene	Gene name	Log_2 fold change	Protein description
VC2465	*rseB*	1.62	Sigma-E factor regulatory protein
VC1403		1.58	Putative methyl-accepting chemotaxis protein
VCA1098		1.57	Putative ABC-type transport system
VCA1090		1.56	Putative chemoreceptor
VCA1101		1.56	Putative ABC-type glutathione transport system ATPase component,
VC0708	*bamD*	1.56	Lipoprotein
VC2600		1.56	Putative membrane-anchored periplasmic protein
VCA1092		1.55	Putative methyl-accepting chemotaxis protein
VC2417	*recJ*	1.54	Exonuclease
VC2464		1.54	Putative Sigma-E factor regulatory protein
VCSEN_ancRNA613		1.53	Small RNA
VC0466		1.52	Putative Holliday junction resolvase
VC0673		1.51	Putative sulfite exporter
VCA0962		1.51	Hypothetical protein
VCA0063	*ptrB*	1.50	Putative Protease
VCA0649		1.50	Conserved hypothetical protein
VCA1089	*cheB*	1.50	Chemotaxis response regulator

Gene	Gene name	Log_2 fold change	Protein description
VC0164	*vexB*	1.50	Bile-regulated RND-family efflux system
VCA0538		1.47	Putative Cytochrome b561
VC1826		1.47	Mannose permease
VCA0849		1.46	Putative T1SS-143 repeat domain protein
VC1576		1.46	Conserved hypothetical protein
VC1400		1.45	Conserved hypothetical protein
VC2212		1.43	Conserved hypothetical protein
VC1217	*hpa2*	1.43	Cutative Histone acetyltransferase
VC1402		1.43	Regulator
VC1044		1.43	Conserved hypothetical protein
VC0580		1.42	Putative endonuclease
VCA0985		1.40	Putative dehydrogenase
VC1872		1.38	Putative serine kinase
VC2366	*rraA*	1.38	Regulator of ribonuclease activity
VCA0908	*hutX*	1.35	Putative heme iron utilization protein
VCA0847		1.33	Putative Amino acid/polyamine transporter
VC0579	*diaA*	1.33	DnaA initiator-associating protein
VC1964		1.31	Putative translocase, subunit

Gene	Gene name	Log_2 fold change	Protein description
VC2732	*epsE*	1.30	General secretion pathway protein
VCA1091		1.30	Putative chemotaxis methyltransferase
VC2419	*xerD*	1.30	Tyrosine recombinase
VCA0551		1.28	Conserved hypothetical protein
VCA0173		1.28	Conserved hypothetical protein
VC1874		1.27	Putative SpoVR family protein
VCA0657	*glpD*	1.27	Glycerol-3-phosphate dehydrogenase
VC0468	*gshB*	1.26	Glutathione synthetase
VC2164		1.25	Putative Zn-dependent protease
VC2733	*epsD*	1.24	General secretion pathway protein
VC0467		1.23	Putative transcriptional regulator
VC1815		1.23	putative cell-cell signaling protein
VC1122		1.22	Cyclopropane-fatty-acyl-phospholipid synthase
VC1379		1.22	Conserved hypothetical protein
VC1575		1.22	Conserved hypothetical protein
VC0165	*vexA*	1.21	Bile-regulated RND-family efflux system
VC0589		1.21	Putative ABC-type multidrug transport system, ATPase component

Gene	Gene name	Log_2 fold change	Protein description
VC1397	*chea-1*	1.21	Signal transduction histidine kinase
VC2724	*epsM*	1.20	General secretion pathway protein
VC2167		1.19	Conserved hypothetical protein
VC2491	*leuB*	1.18	3-Isopropylmalate dehydrogenase
VC1484	*rmf*	1.18	Ribosome modulation factor
VC1252		1.17	Putative competence/damage-inducible protein
VC1642		1.17	Putative ribosome recycling factor
VCA0216		1.17	Conserved hypothetical protein
VC2726	*epsK*	1.16	General secretion pathway protein
VC0578	*osmY*	1.15	Putative periplasmic or secreted lipoprotein
VC2165		1.15	Putative arsenate reductase
VC0590		1.15	Putative ABC-type multidrug transport system, permease component
VC2731	*epsF*	1.12	General secretion pathway protein
VCA0167		1.11	Conserved hypothetical protein
VC2725	*epsL*	1.11	General secretion pathway protein
VCA0853		1.10	Putative Outer membrane lipoprotein-sorting protein
VC1117	*htpX*	1.09	Heat shock protein

Gene	Gene name	Log_2 fold change	Protein description
VCA0744	*glpK*	1.08	Glycerol kinase
VC0470	*dns*	1.08	Extracellular deoxyribonuclease
VC2729	*epsH*	1.07	General secretion pathway protein
VC2728	*exeI*	1.07	General secretion pathway protein
VC2730	*epsG*	1.06	General secretion pathway protein
VCA0539		1.06	Putative YceI-like domain protein
VCA0241	*sgbU*	1.05	Putative L-ribulose-5-phosphate 3-epimerase
VC0818		1.05	Transposase
VC2166		1.05	Quinone oxidoreductase
VCA0989	*vcmN*	1.04	Multidrug efflux pump
VC2251	*ompH*	1.03	Putative Outer membrane chaperone
VC1236	*msrB*	1.02	Sulfoxide reductase
VC0885		1.02	Conserved hypothetical protein

Table 2.2 Downregulated transcripts in wild-type cells grown in LB with and without polymyxin B.

Gene	Gene name	Log_2 fold change	Protein description
VC2305	*ompK*	-1.02	Outer membrane protein
VCA0344		-1.02	conserved hypothetical protein
VC1835		-1.03	lipoprotein
VCt015		-1.04	tRNA
VCA1065		-1.09	conserved hypothetical protein
VCt021		-1.22	tRNA-Met
VC0162	*ilvC*	-1.29	Keto-acid reductoisomerase
VCt071		-1.30	tRNA-Leu
VC1415	*hcp1*	-1.35	Type VI secretion effector
VCt058		-1.38	tRNA-Leu
VCA0017	*hcp2*	-1.40	Type VI secretion effector
VC0633	*ompU*	-1.47	Outer membrane protein
VC2213	*ompA*	-1.49	Outer membrane protein
VC2361	*grcA*	-1.49	glycyl radical cofactor
VC0156	*btuB*	-1.50	Outer membrane vitamin receptor
VCt073		-1.87	tRNA-Leu
VC0828	*tcpA*	-2.10	Toxin coregulated pilin
VC1854	*ompT*	-2.44	Outer membrane porin

2.3.2. Genome-wide screen reveals membrane biogenesis and lipid A modification are important for fitness in the presence of polymyxin B

To identify *V. cholerae* genes that contribute to fitness when cells are grown under sub-MIC concentrations of polymyxin B, a randomly barcoded transposon mutant library was used, followed by randomly barcoded transposon sequencing (RB-TnSeq). We grew the wild-type *V. cholerae* randomly barcoded library in the presence and absence of ½ MIC of polymyxin B, with exposure for two passages. Samples were collected and then sequenced to determine DNA-barcode abundance in the presence and absence of polymyxin B (Figure 2.2A). A unique barcode insertion results in a unique mutant with a DNA barcode distributed across two chromosomes in the *V. cholerae* genome (Figure 2.2B); these insertions occur in non-essential genes. The RB-TnSeq experiment identified 3,347 genes with insertions out of 3,765 protein-encoding genes in the *V. cholerae* genome (Table 2.3). The significance threshold was met with a |log2(fitness)| greater than or equal to 1 and a |t-like test statistic| greater than or equal to 3 (Figure 2.2C). A total of 57 genes with insertions resulted in significant fitness differences: 46 decreased fitness and 11 increased fitness in the presence of polymyxin B (Table 3). Genes with significant fitness differences were grouped into four categories: CarR regulon (pink), lipopolysaccharide biogenesis (green), outer membrane biogenesis (purple), and previously uncharacterized genes in *V. cholerae* (orange) (Figure 2.2 C). The 4 most significant (padj < 0.05) pathways are as follows, electron transport and respiration and DNA repair and recombination with positive NES, interpreted as genes whose absence results in increased fitness in the presence of polymyxin B. Envelope stress response pathway with a negative NES and Lipopolysaccharide biosynthesis with the most negative NES, indicating genes whose absence results in decreased fitness in the presence of polymyxin B (Figure 2.2D).

Figure 2.2. Mutants contributing to fitness differences in the presence of polymyxin B in wild-type *V. cholerae* randomly barcoded transposon mutant library grown in LB with or without the presence of polymyxin B.

Mutant strain abundance was quantified by DNA barcode abundance in the presence of polymyxin B compared to the LB media control. A) Workflow of the library generation and Barseq experiment. B) Map of the unique insertions in chromosomes 1 and 2 in the *V. cholerae* genome. C) Volcano plot displays genes contributing to fitness differences. The t-like test statistic is plotted on the y-axis, and the log of the fold-change (FC) (base 2) is plotted on the x-axis. Each point represents a mutant with a unique barcode. Mutants were grouped into the CarR regulon (pink), LPS biogenesis (green), membrane proteins (purple), and other proteins (orange). Grey lines indicate fitness cutoffs: a $\log_2$ fold-change greater than 1 (vertical lines) and a t-like test statistic greater than 3 (horizontal line). A $\log_2$ fold-change less than 1 indicates decreased fitness in the mutant compared to WT, and a log2 fold-change greater than 1 indicates increased fitness in the mutant compared to WT. D) GSEA bubble plot displaying the 4 most significant pathways; Normalized Enrichment Score (NES): positive means enriched among upregulated/ benefit genes, and negative means enriched among downregulated genes/cost genes. Dot size represents the number of leading-edge genes driving enrichment, and dot color represents the -log10(adjusted p-value); lighter green indicates greater significance.

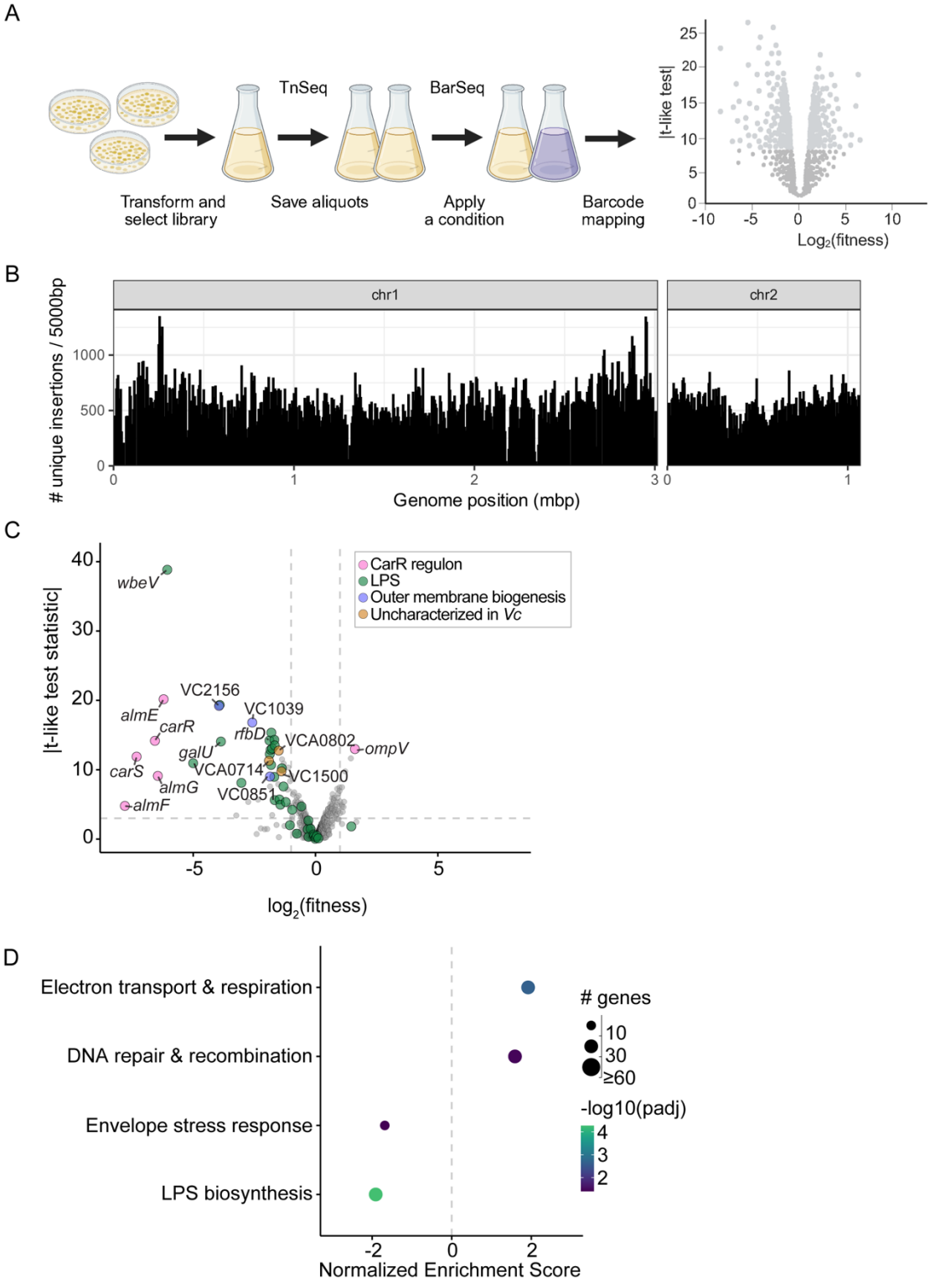
A
TnSeq
BarSeq
Transform and select library
Save aliquots
Apply a condition
Barcode mapping
|t-like test|
Log2(fitness)
B
chr1
chr2
unique insertions / 5000bp
Genome position (mbp)
C
CarR regulon
LPS
Outer membrane biogenesis
Uncharacterized in Vc
|t-like test statistic|
log2(fitness)
wbeV
VC2156
VC1039
almE
carR
rfbD
VCA0802
ompV
galU
carS
VCA0714
VC1500
almG
VC0851
almF
D
Electron transport & respiration
DNA repair & recombination
Envelope stress response
LPS biosynthesis
Normalized Enrichment Score
genes
10
30
≥60
-log10(padj)
4
3
2

Table 2.3 Genes contributing to fitness differences in the presence of polymyxin B

Gene	Gene name	Log_2 fold change	t-like test	Protein description
VC1578	*almF*	-7.79	-4.78	Glycine-carrier protein
VC1319	*carS*	-7.31	-11.89	Sensor histidine kinase
VC1320	*carR*	-6.56	-14.17	Response regulator
VC1577	*almG*	-6.45	-9.11	Glycyltransferase
VC1579	*almE*	-6.21	-20.17	Aminoacyl-adenyltransferase carrier
VC0260	*wbeV*	-6.06	-38.84	Mannosyl-transferase
VC0224	*KdtX*	-5.00	-10.94	Lipopolysaccharide biosynthesis glycosyltransferase
VC2156		-3.94	-19.20	Lipoprotein, assembly factor C
VC0239	*wavL*	-3.92	-19.35	Glycosyltransferase
VC0395	*galU*	-3.87	-14.07	UDP-glucose-pyrophosphorylase
VC0576	*sspA*	-3.24	-3.40	Stringent starvation protein A
VC0212	*lpxN*	-3.03	-8.11	Lipid A secondary hydroxyl-acyltransferase
VC0761		-2.75	-5.36	Conserved hypothetical protein
VC1039		-2.59	-16.81	AsmA-domain protein
VC1887	*csiV*	-2.35	-5.70	Putative TPR protein
VCA0714		-1.90	-11.29	Diacylglycerol kinase
VC0243	*rfbD*	-1.88	-14.21	Oxidoreductase

Gene	Gene name	Log_2 fold change	t-like test	Protein description
VC0245	*rfbG*	-1.87	-12.25	Glycosyltransferase
VC0851	*smpA*	-1.86	-9.0	Small protein
VC0346		-1.86	-7.59	tRNA dimethylallytransferase
VC0249	*rfbL*	-1.84	-12.87	Acyl-CoA synthetase
VC0252	*rfbO*	-1.82	-10.69	Galactoside O-acetyltransferase
VC0251		-1.81	-15.35	Acyl-protein synthetase
VC0250		-1.77	-13.05	Dehydrogenase
VC2466	*rseA*	-1.77	-3.46	Sigma-E factor negative regulatory protein
VC0259	*wbeU*	-1.69	-8.96	Glycosyltransferase
VC0241	*rfbA*	-1.68	-14.31	Mannose-1-phosphate guanylyltransferase
VC0242	*rfbB*	-1.67	-13.51	Phosphomannomutase
VC0237	*waaL*	-1.67	-5.62	O-antigen ligase
VC0269	*manA*	-1.65	-14.37	Mannose-6-phosphate isomerase
VC2604	*slyD*	-1.53	-7.91	Peptidyl-prolyl cis-trans isomerase
VCA0802		-1.51	-12.76	Conserved hypothetical
VC0247	*rfbI*	-1.48	-5.71	Lipopolysaccharide/O-antigen transport ATPase
VC0246	*rfbH*	-1.44	-4.96	Lipopolysaccharide/O-antigen transport permease
VC1500		-1.39	-9.76	Paraquat-inducible protein

Gene	Gene name	Log_2 fold change	t-like test	Protein description
VC0244	*rfbE*	-1.38	-10.21	Perosamine synthase
VC2436	*tolC*	-1.37	-11.50	Outer membrane efflux protein
VC1965		-1.35	-10.13	Conserved hypothetical
VC0235	*wavJ*	-1.31	-7.58	Lipopolysaccharide biosynthesis protein
VC1501		-1.30	-10.88	Hypothetical transcriptional regulator
VC0263	*wbeW*	-1.22	-5.34	Galactosyl-transferase
VC1894	*lpoB*	-1.14	-7.14	Lipoprotein
VC2600	VC2600	-1.12	-10.32	Conserved hypothetical
VC1179	*rluB*	-1.08	-4.82	Pseudouridylate synthase
VC0566	*degP*	-1.04	-8.36	Protease
VC0941	*glyA*	1.01	5.43	Serine hydroxylmethyltransferase
VC0055	*hemF*	1.01	3.75	Coproporphyrinogen oxidase
VC2522		1.08	4.92	Ca^{2+}/Na^{+} antiporter
VC0547	*lysC*	1.08	7.48	Aspartokinase
VC2292	*nqrD*	1.09	4.68	Ubiquinone oxidoreductase
VC1922	*clpP*	1.11	3.94	Protease
VC2288		1.14	4.63	Conserved hypothetical
VC2040		1.17	5.38	Conserved hypothetical
VC0274		1.21	9.77	Hypothetical protein

Gene	Gene name	Log_2 fold change	t-like test	Protein description
VC2749	*glnG*	1.44	11.64	Nitrogen regulation protein
VC1318	*ompV*	1.61	12.99	Outer membrane protein

2.3.3. CarRS two-component signal transduction system and envelope stress-related genes overlap between the RNA-seq and RB-TnSeq experiments

We compared the outputs of the RNA-seq and RB-TnSeq experiments. From the RNA-seq and RB-TnSeq, only 9 genes overlap and meet the full differential thresholds: log2(fold-change) > 1 and adjusted $p < 0.05$ for RNA-seq, and t-like test statistic $>|\geq 3$ for BarSeq (Figure 2.3A). The genes identified include *carR*, *car*S, regulon members *almEFG* and *ompV*, along with two envelope-related genes, *degP* (VC0566), a predicted protease (21), *rseA* (VC2466), a gene encoding a Sigma-E negative regulatory protein (22), and VC2600, encoding a conserved hypothetical protein (Table 2.4). Using adjusted RNA-seq thresholds of $p < 0.05$, without accounting for differential abundance, and BarSeq together increase the number of overlapping genes to 38, as shown in a heatmap of genes overlapping between the BarSeq and RNA-seq experiments (Figure 2.3B). The limited overlap between genes found in these experiments indicates that not all genes differentially regulated by polymyxin B exposure are essential for fitness, and that genes critical for polymyxin B fitness may not be transcriptionally regulated under our experimental conditions.

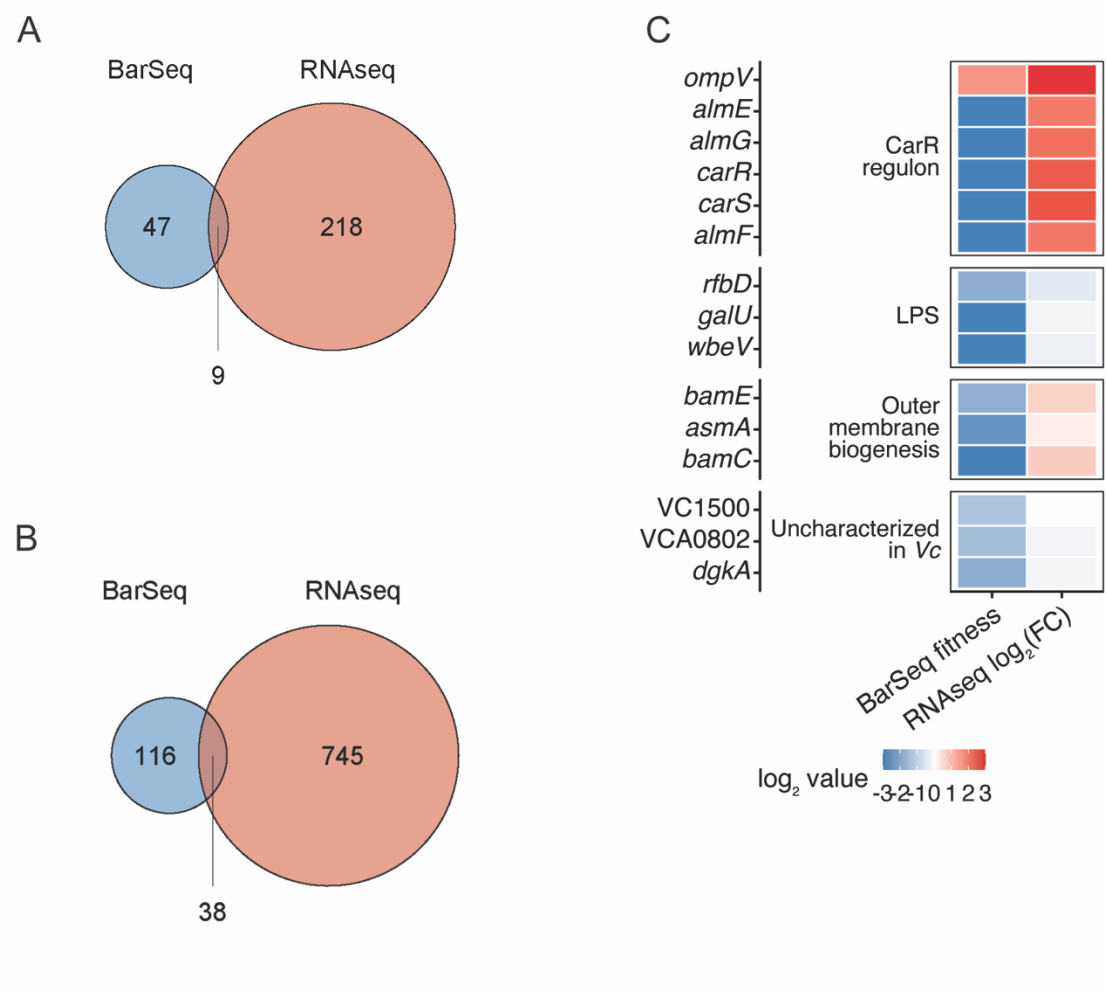

Figure 2.3. Genes regulated and contributing to fitness differences in the presence of polymyxin B

Venn diagram of overlap between differentially regulated genes in the RNA-seq (polymyxin B vs LB) and BarSeq (polymyxin B fitness) datasets. A) Venn diagram of overlapping genes meeting full differential thresholds $|\log_2 \text{(fold-change)}| \geq 1$ and adjusted $p \leq 0.05$ for RNA-seq and $|\text{t-like test statistic}| \geq 3$ for BarSeq. B) Venn diagram of overlapping genes meeting the significance threshold Gene/transcripts with adjusted $p \leq 0.05$ in RNA-seq and BarSeq. C) Heat map view identifying genes overlapping in BarSeq (left column) and RNA-seq (right column). Each panel represents the grouped genes. Blue represents decreased fitness and red represents increased fitness in BarSeq; blue represents downregulation and red represents upregulation in RNA-seq.

Table 2.4 Genes overlapping in the RNA-seq and Barseq

Gene	Gene name	Log_2 fold change	t-like test	Log_2 fold change	Protein description
VC1578	*almF*	-7.79	-4.78	2.08	Glycine-carrier protein
VC1319	*carS*	-7.31	-11.89	2.61	Sensor histidine kinase
VC1320	*carR*	-6.56	-14.17	2.51	Response regulator
VC1577	*almG*	-6.45	-9.11	2.20	Glycyltransferase
VC1579	*almE*	-6.21	-20.17	2.04	Aminoacyl-adenyltransferase carrier
VC2466	*rseA*	-1.77	-3.46	2.04	Sigma-E factor negative regulatory protein
VC2600	VC2600	-1.12	-10.32	1.56	Predicted hydrolase
VC0566	*degP*	-1.04	-8.36	2.74	Protease
VC1318	*ompV*	1.61	12.99	3.44	Outer membrane protein

2.3.4. CarRS two-component signal transduction system and CarR regulon contribute to fitness in the presence of polymyxin B

Bar-Seq analysis identified previously known genes important for polymyxin B, which we expected to be important fitness determinants. These included the CarRS TCS system and CarR regulon members. The CarR regulon members are the three-gene operon *almEFG* and the *ompV* gene. *carR* (VC1320) *encodes* a response regulator, and *carS* (VC1319) encodes a sensor histidine kinase (11). *almE* (VC1579) encodes a dual aminoacyl-adenyltransferase/carrier protein ligase; *almF* (VC1578) encodes a glycine-carrier protein (23); and *almG* (VC1577) encodes a glycyltransferase (24). *ompV* (VC1318) encodes the outer membrane porin (12). Transposon insertions in *carR*, *carS*, *almE*, *almF*, and *almG* resulted in strong fitness defects, with fitness scores ranging from -6.21 to -7.31. Specifically, insertions in *carR* and *carS* reduced fitness by -6.56 and -7.31, respectively, while insertions in *almE*, *almF*, and *almG* reduced fitness by -6.21, -7.31, and -6.45. In contrast, insertion in *ompV* increased fitness (1.61) (Table 2.3).

To confirm the fitness defects identified in the Bar-seq screen, we generated individual deletion mutants and performed in vitro competitive index assays in the presence of polymyxin B. We found that Δ*carR*, Δ*carS*, and Δ*almEFG* mutants were outcompeted by the wild type in the presence of polymyxin B. We determined this because no mutant cells were detected after 24 hours of competition. In contrast, the Δ*ompV* mutant outcompeted the wild type under the same conditions, consistent with its increased fitness as indicated by the Barseq results (Figure 2.4B). This finding was unexpected, as OmpV has been proposed as an outer membrane-localized polymyxin B sensor that activates the CarRS TCS system (18). This finding needs confirmation through complementation analysis and by ensuring that the *ompV* mutant did not accumulate mutations, that the mutation is not polar, and that it has no unintended consequences.

In the MIC assay, deletion of *carR*, *carS*, *almE*, *almF*, and *almG* markedly reduced polymyxin B resistance. The average MIC values were 4.5 μg/ml for Δ*carR* and Δ*carS* and 3.5-3.8 μg/ml for Δ*almE*, Δ*almF*, and Δ*almG*, compared with wild type at 43 μg/ml. In contrast, the Δ*ompV* mutant at 48 μg/ml showed resistance like wild type at 43 μg/ml (Figure 2.4C).

Consistent with the Tn-seq results and published studies, Δ*carR*, Δ*carS*, and Δ*almEFG* mutants failed to grow in the presence of polymyxin B, indicating that these genes are required for polymyxin B resistance. In contrast, the Δ*ompV* mutant exhibited enhanced growth in the presence of polymyxin B. None of the mutants exhibited growth defects relative to the wild type under untreated conditions, indicating that the observed phenotypes are specific to polymyxin B exposure (Figure 2.4D).

Figure 2.4. The CarRS TCS and CarR regulon members are key determinants of polymyxin B fitness

A) Volcano plot displays genes contributing to fitness differences in the *V. cholerae* genome. The t-like test statistic is plotted on the y-axis, and the log of the fold-change (FC) (base 2) is plotted on the x-axis. Each point represents a mutant with a unique barcode. Grey lines indicate fitness cutoffs: a $\log_2$ fold-change greater than 1 (vertical lines) and a t-like test statistic greater than 3 (horizontal line). A $\log_2$ fold-change less than 1 indicates decreased fitness in the mutant compared to WT, and a log2 fold-change greater than 1 indicates increased fitness in the mutant compared to WT. Pink indicates the mutants identified as part of the CarR regulon: *carR*, *carS*, *almE*, *almF*, *almG*, and *ompV*. B) A plot of relative fitness measured by in vitro competition of mutants against the wild-type strain competed for 24hours. Relative fitness was measured by in vitro competition of mutants against the wild-type strain for 24 hours. Competitive index (CI) values are plotted on a log10 scale. Means from ≥ 3 independent biological replicates were compared to WT by one-way ANOVA followed by Dunnett's multiple comparison test. Statistical comparisons were performed on log10(CI) values. Mean differences with an adjusted *P* value of ≤ 0.01 were deemed significant. *, $P \leq 0.01$; **, $P \leq 0.001$; ***, $P \leq 0.0001$; ns, not significant. Strains for which no colonies were recovered at the detection limit are indicated as ND (not detected) and were excluded from statistical comparisons. C) Bar graph of polymyxin B resistance quantification of MIC for Δ*carR*, Δ*carS*, Δ*almE*, Δ*almF*, Δ*almG*, and Δ*ompV* mutants. Statistical analysis, n=3 biological replicates, one-way ANOVA to compare means of mutants to WT followed by Dunnett's multiple comparison test. ***$p < 0.0001$. D) Growth curves of mutants compared WT in the presence and absence of polymyxin B. Black lines refer to WT and pink lines represent the respective mutant; solid lines represent growth in LB and dashed lines represent growth in the presence of polymyxin B, with n=3 biological replicates

.

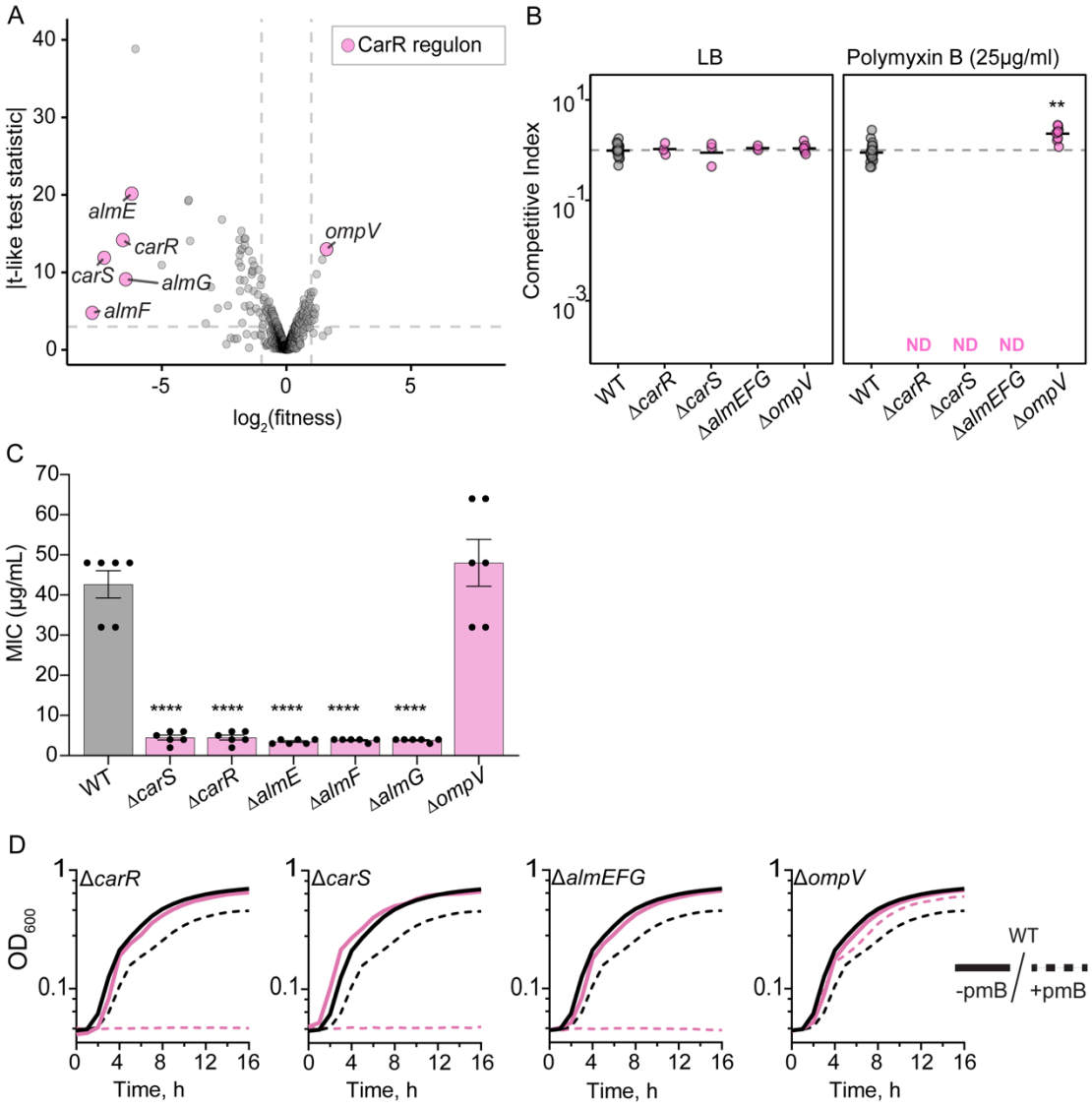
A
CarR regulon
|t-like test statistic|
log2(fitness)
almE
carR
carS
almG
almF
ompV
B
LB
Polymyxin B (25μg/ml)
Competitive Index
ND
ND
ND
**
WT
ΔcarR
ΔcarS
ΔalmEFG
ΔompV
C
MIC (μg/mL)
****
WT
ΔcarS
ΔcarR
ΔalmE
ΔalmF
ΔalmG
ΔompV
D
ΔcarR
ΔcarS
ΔalmEFG
ΔompV
OD600
Time, h
WT
-pmB
+pmB

2.3.5. Lipopolysaccharide biogenesis genes

Lipopolysaccharide biosynthesis genes were the most numerous to be absent, resulting in significantly decreased fitness (Table 2.3). LPS is composed of lipid A, the core, and the O-antigen. To characterize the impact of lipopolysaccharide biosynthesis genes, representative genes were selected based on their roles in LPS biogenesis: *wbeV* (VC0260), *galU* (VC0395), and *rfbD* (VC0243). *wbeV* encodes a mannosyltransferase involved in O-antigen biosynthesis. *galU* encodes UDP-glucose-pyrophosphorylase, which catalyzes the biosynthesis of UDP-glucose, an essential building block of the LPS core oligosaccharide and extracellular polysaccharides utilized for outer membrane biogenesis (25). *rfbD* encodes an oxidoreductase that converts GDP-mannose to GDP-4-keto-6-deoxymannose, thereby synthesizing the perosamine sugar, which is important for the formation of the repeating O-antigen unit backbone of LPS (26).

Transposon insertions in *wbeV*, *galU*, and *rfbD* resulted in significant fitness defects in the presence of polymyxin B (Figure 2.5A). Insertions in *wbeV*, g*alU*, and r*fbD* reduced fitness by -6.06, -3.87, and -1.88, respectively (Table 2.3). To confirm these findings, individual deletion mutants were constructed, and their fitness following polymyxin B exposure was assessed. In the in vitro competition assay, Δ*wbeV* competed similarly to the wild type in the presence of polymyxin B. In contrast, Δ*galU* and Δr*fbD* were outcompeted by the wild type after 24 hours of competition (Figure 2.5B). We also observed a difference in the LB media for the Δ*galU* and Δr*fbD* mutants, we expect to see this as these mutants are part of the core-LPS structure of the outer membrane. The observed phenotypes were complemented by expressing WbeV, GalU, or RfbD from the pMMB67EH plasmid under the control of the inducible Ptac promoter, restoring fitness to wild type levels (Figure 2.5C). For the complementation, additional replicates will be performed to obtain 3 biological replicates, and statistics will be corrected.

In the MIC assay, the average MIC values were 32 µg/ml for Δ*wbeV*, 2.5 µg/ml for Δg*alU*, and 8 µg/ml for Δr*fbD*, compared with 43 µg/ml for wild type (Figure 2.5D). Consistent with these MIC values, Δg*alU* failed to grow in the presence of polymyxin B, while the growth of Δ*rfbD* was substantially impaired. In contrast, Δ*wbeV* exhibited growth comparable to that observed in the absence of polymyxin B (Figure 2.5B). None of the mutants displayed growth defects relative to the wild type in the presence of polymyxin B (Figure 2.5E). Taken together, these results suggest that LPS production and altered LPS composition affect polymyxin B sensitivity, possibly due to changes in B binding to lipid A. These findings also suggest that genes conferring polymyxin B fitness may not exhibit observable growth defects at sub-MIC levels of polymyxin B.

Figure 2.5. Lipopolysaccharide biosynthesis genes impact polymyxin B fitness
A) Volcano plot displays genes contributing to fitness differences in the *V. cholerae* genome. The t-like test statistic is plotted on the y-axis, and the log of the fold-change (FC) (base 2) is plotted on the x-axis. Each point represents a mutant with a unique barcode. Grey lines indicate fitness cutoffs: a $\log_2$ fold-change greater than 1 (vertical lines) and a t-like test statistic greater than 3 (horizontal line). A $\log_2$ fold-change less than 1 indicates decreased fitness in the mutant compared to WT, and a log2 fold-change greater than 1 indicates increased fitness in the mutant compared to WT. Green indicates mutants identified as LPS biogenesis genes: *wbeV*, *galU*, and *rfbD.* B) A plot of relative fitness measured by in vitro competition of deletion mutants against the WT; deletion mutants competed against the WT strain for 24hours. Competitive index (CI) values are plotted on a log10 scale. Means from ≥ 3 independent biological replicates were compared to WT by one-way ANOVA followed by Dunnett's multiple comparison test. Statistical comparisons were performed on log10(CI) values. Mean differences with an adjusted *P* value of ≤ 0.01 were deemed significant. *, $P \leq 0.01$; **, $P \leq 0.001$; ***, $P \leq 0.0001$; ns, not significant. Strains for which no colonies were recovered at the detection limit are indicated as ND (not detected) and were excluded from statistical comparisons. C) A plot of relative fitness measured by in vitro competition of WT with gene of interest, complemented, mutant with empty vector against the WT strain; WT with empty vector; competed for 24hours. Competitive index (CI) values are plotted on a log10 scale. Means from ≥ 1 independent biological replicate were compared to WT by one-way ANOVA followed by Dunnett's multiple comparison test. Statistical comparisons were performed on log10(CI) values. Mean differences with an adjusted *P* value of ≤ 0.01 were deemed significant. *, $P \leq 0.01$; **, $P \leq 0.001$; ***, $P \leq 0.0001$; ns, not significant. Strains for which no colonies were recovered at the detection limit are indicated as ND (not detected) and were excluded from statistical comparisons. D) Bar graph of polymyxin B resistance quantification of MIC for Δ*wbeV*, Δ*galU*, and Δ*rfbD* mutants. Statistical analysis, n=3 biological replicates, one-way ANOVA to compare means of mutants to WT followed by Dunnett's multiple comparison test. $^{**}p < 0.003$ and $^{***}p < 0.0001$. E) Growth curves of mutants compared to WT in the presence and absence of polymyxin B. Black lines refer to WT, and the green line represents the respective mutant; solid lines represent growth in LB and dashed lines represent growth in the presence of polymyxin B, with n=3 biological replicates.

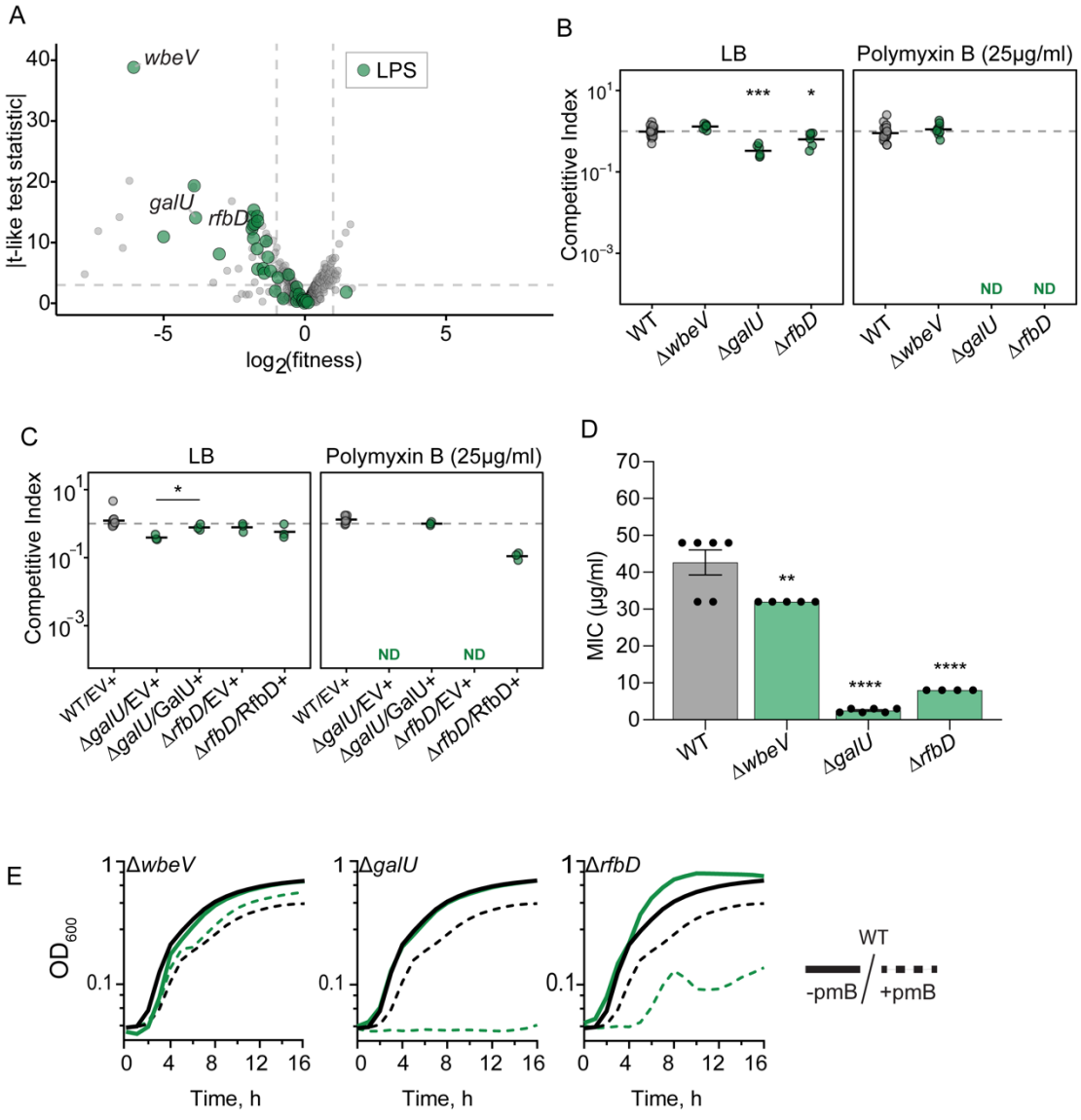
A
wbeV
galU
rfbD
LPS
|t-like test statistic|
log2(fitness)
B
LB
Polymyxin B (25µg/ml)
Competitive Index
***
*
ND
ND
WT
ΔwbeV
ΔgalU
ΔrfbD
C
LB
Polymyxin B (25µg/ml)
Competitive Index
*
ND
ND
WT/EV+
ΔgalU/EV+
ΔgalU/GalU+
ΔrfbD/EV+
ΔrfbD/RfbD+
D
MIC (µg/ml)
**
****
****
WT
ΔwbeV
ΔgalU
ΔrfbD
E
ΔwbeV
ΔgalU
ΔrfbD
OD600
Time, h
WT
-pmB
+pmB

2.3.6. Outer membrane biogenesis genes impact fitness in response to polymyxin B

Our screen identified a set of genes predicted to be involved in outer membrane biogenesis whose functions have not been experimentally tested in *V. cholerae*. These include VC1039, which encodes an AsmA-domain-containing protein predicted to be involved in lipid transfer for outer membrane biogenesis (27); VC0851, which encodes a small lipoprotein A predicted to be the homolog of the outer membrane protein assembly factor BamE; and VC2156, which encodes a lipoprotein predicted to be an outer membrane protein assembly factor BamE (28). Transposon insertions in VC1039, VC0851, and VC2156 resulted in significant fitness defects during polymyxin B exposure (Figure 2.6A). Insertions in VC1039 reduced fitness by -2.59, while insertions in VC0851 and VC2156 reduced fitness by -1.87 and -3.9, respectively (Table 2.3). In the in vitro competitive assay, ΔVC1039 was outcompeted by the wild type after 24 hours of competition in the presence of polymyxin B, indicating a fitness defect under these conditions. In contrast, ΔVC0851 competed similarly to the wild type in the presence of polymyxin B (Figure 2.6B). Expression of VC1039 or VC0851 from the pMMB67EH plasmid under the control of the inducible Ptac promoter complemented the corresponding mutant phenotypes (Figure 2.6C). In the MIC assay, the average polymyxin B MIC was 32 μg/ml for ΔVC1039, ΔVC0851, and ΔVC2156 compared to 43 μg/ml for wild type. Growth in the presence of polymyxin B, ΔVC1039, ΔVC0851 and ΔVC2156 was not affected compared to the wild type (Figure 2.6D). None of the three mutants showed growth defects compared to wild type in the absence of polymyxin B (Figure 2.6E).

Taken together, these findings suggest that OM biogenesis, BAM protein assembly machinery, and lipid transport contribute to CAMP fitness in *V. cholerae*. We further explored VC1039, as this gene has not been characterized in *V. cholerae* previously. We aimed to identify VC1039 conservation at the genus level and distantly related orthologs but found none. The closest orthologs found at the genus level were in *Vibrio furnissii*, *Vibrio*

anguillarum, *Vibrio parahaemolyticus*, *Vibrio vulnificus*, and *Vibrio fluviallis*. Distantly related orthologs found in *Allivibrio logei*, *Photobacterium sp*., *Escherichia coli*, and *Pseudomonas aeruginosa* show VC1039's protein conservation across evolutionary distance (Figure 2.7).

Figure 2.6. Outer membrane biogenesis genes play a role in polymyxin B response
A) Volcano plot displays genes contributing to fitness differences in the *V. cholerae* genome. The t-like test statistic is plotted on the y-axis, and the log of the fold-change (FC) (base 2) is plotted on the x-axis. Each point represents a mutant with a unique barcode. Grey lines indicate fitness cutoffs: a $\log_2$ fold-change greater than 1 (vertical lines) and a t-like test statistic greater than 3 (horizontal line). A $\log_2$ fold-change less than 1 indicates decreased fitness in the mutant compared to WT, and a log2 fold-change greater than 1 indicates increased fitness in the mutant compared to WT. Purple color indicates the mutants identified as membrane-associated genes: VC1039, VC2156, and VC0851. B) A plot of relative fitness measured by in vitro competition of deletion mutants against the WT strain competed for 24hours. Competitive index (CI) values are plotted on a log10 scale. Means from ≥ 3 independent biological replicates were compared to WT by one-way ANOVA followed by Dunnett's multiple comparison test. Statistical comparisons were performed on log10(CI) values. Mean differences with an adjusted *P* value of ≤ 0.01 were deemed significant. *, $P \leq 0.01$; **, $P \leq 0.001$; ***, $P \leq 0.0001$; ns, not significant. Strains for which no colonies were recovered at the detection limit are indicated as ND (not detected) and were excluded from statistical comparisons. C) A plot of relative fitness measured by in vitro competition of WT with gene of interest, complement, mutant with empty vector against the WT strain; WT with empty vector; competed for 24hours. Competitive index (CI) values are plotted on a log10 scale. Means from ≥ 1 independent biological replicate were compared to WT by one-way ANOVA followed by Dunnett's multiple comparison test. Statistical comparisons were performed on log10(CI) values. Mean differences with an adjusted *P* value of ≤ 0.01 were deemed significant. *, $P \leq 0.01$; **, $P \leq 0.001$; ***, $P \leq 0.0001$; ns, not significant. Strains for which no colonies were recovered at the detection limit are indicated as ND (not detected) and were excluded from statistical comparisons. D) Bar graph of polymyxin B resistance quantification of MIC for ΔVC1039, ΔVC0851, and ΔVC2156 mutants. Statistical analysis, n=3 biological replicates, one-way ANOVA to compare means of mutants to WT followed by Dunnett's multiple comparison test. $^{**}p < 0.003$ and $^{***}p < 0.0001$. E) Growth curves of mutants compared to WT in the presence and absence of polymyxin B. Black lines refer to WT and the purple line represents the respective mutant; solid lines represent growth in LB and dashed lines represent growth in the presence of polymyxin B, with n=3 biological replicates.

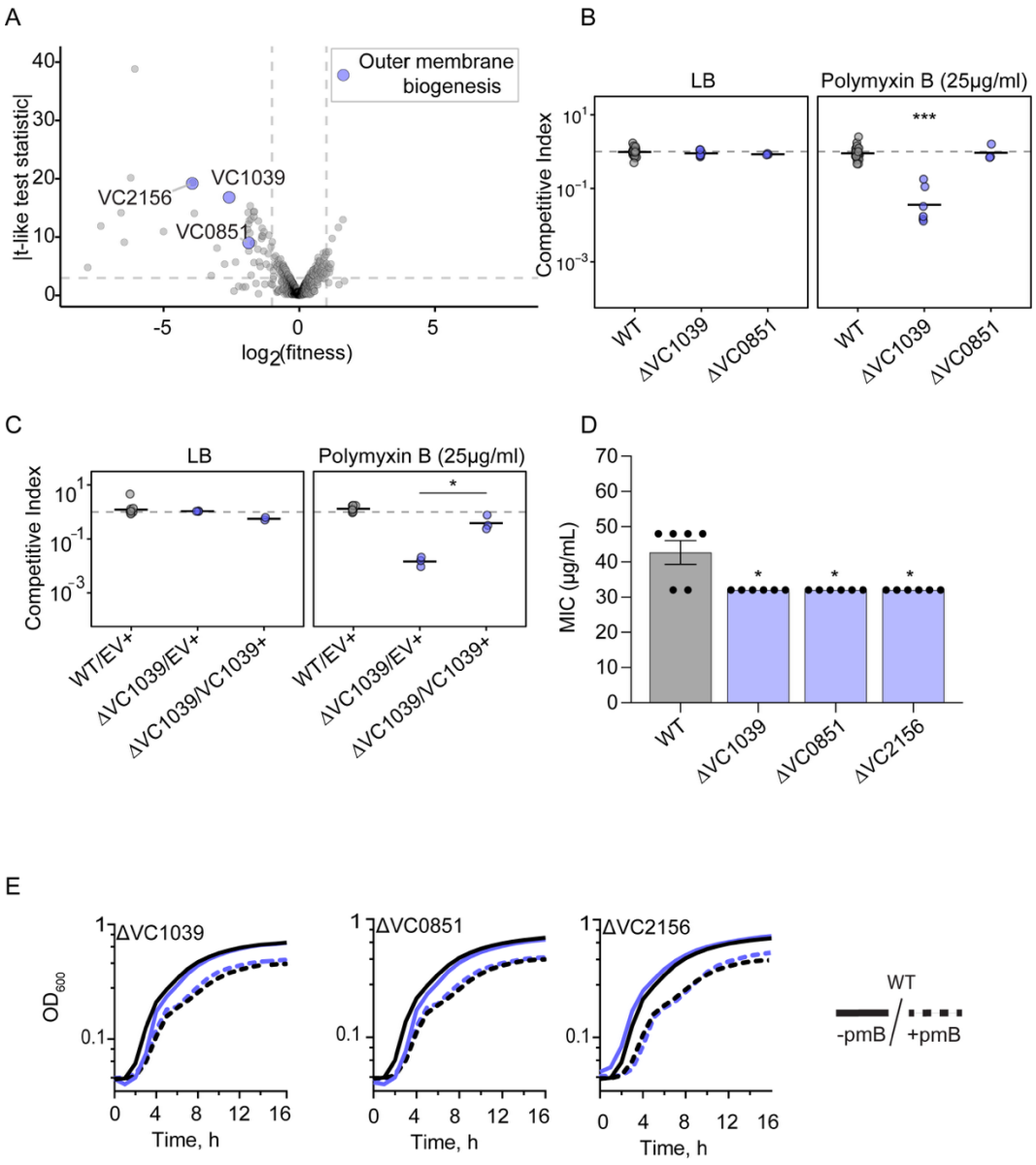
A
Outer membrane biogenesis
VC1039
VC2156
VC0851
|t-like test statistic|
log2(fitness)
B
LB
Polymyxin B (25μg/ml)
Competitive Index
***
WT
ΔVC1039
ΔVC0851
C
LB
Polymyxin B (25μg/ml)
Competitive Index
*
WT/EV+
ΔVC1039/EV+
ΔVC1039/VC1039+
D
MIC (μg/mL)
WT
ΔVC1039
ΔVC0851
ΔVC2156
E
ΔVC1039
ΔVC0851
ΔVC2156
OD600
Time, h
WT
-pmB
+pmB

Figure 2.7. Alignment of VC1039 and representative orthologs
VC1039 orthologs were identified using the EggNOG orthology database to span the range of taxonomic distances from *Vibrio cholerae* O1 biovar El Tor str. A1552, prioritizing sequences with 35-85% identity to the query within each taxonomic group and excluding fragmentary sequences (<50% of query length). The closest same-genus relatives are *Vibrio furnissii*, *Vibrio anguillarum*, *Vibrio parahaemolyticus*, *Vibrio vulnificus*, and *Vibrio fluviallis*. Distantly related orthologs in *Allivibrio logei*, *Photobacterium sp*., *Escherichia coli*, and *Pseudomonas aeruginosa* show protein conservation across evolutionary distance. We aligned sequences using MAFFT v7.526 (L-INS-i) and visualized them with pyMSAviz v5.0; we performed no trimming.

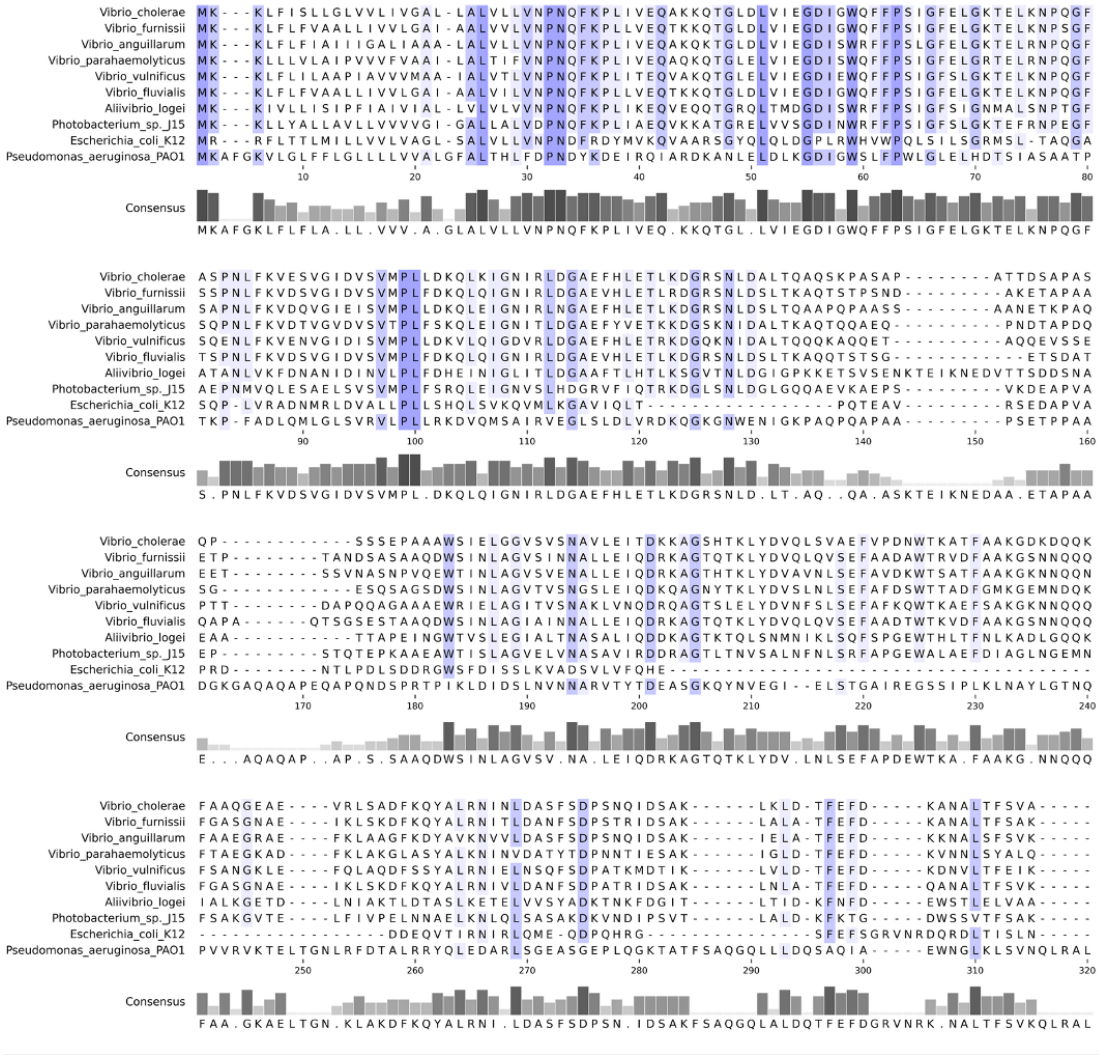
Vibrio_cholerae
Vibrio_furnissii
Vibrio_anguillarum
Vibrio_parahaemolyticus
Vibrio_vulnificus
Vibrio_fluvialis
Aliivibrio_logei
Photobacterium_sp._J15
Escherichia_coli_K12
Pseudomonas_aeruginosa_PAO1
Consensus
MKAFGKLFLFLA.LL.VVV.A.GLALVLLVNPNQFKPLIVEQ.KKQTGL.LVIEGDIGWQFFPSIGFELGKTELKNPQGF

Vibrio_cholerae
Vibrio_furnissii
Vibrio_anguillarum
Vibrio_parahaemolyticus
Vibrio_vulnificus
Vibrio_fluvialis
Aliivibrio_logei
Photobacterium_sp._J15
Escherichia_coli_K12
Pseudomonas_aeruginosa_PAO1
Consensus
S.PNLFKVDSVGIDVSVMPL.DKQLQIGNIRLDGAEFHLETLKDGRSNLD.LT.AQ..QA.ASKTEIKNEDAA.ETAPAA

Vibrio_cholerae
Vibrio_furnissii
Vibrio_anguillarum
Vibrio_parahaemolyticus
Vibrio_vulnificus
Vibrio_fluvialis
Aliivibrio_logei
Photobacterium_sp._J15
Escherichia_coli_K12
Pseudomonas_aeruginosa_PAO1
Consensus
E...AQAQAP..AP.S.SAAQDWSINLAGVSV.NA.LEIQDRKAGTQTKLYDV.LNLSEFAPDEWTKA.FAAKG.NNQQQ

Vibrio_cholerae
Vibrio_furnissii
Vibrio_anguillarum
Vibrio_parahaemolyticus
Vibrio_vulnificus
Vibrio_fluvialis
Aliivibrio_logei
Photobacterium_sp._J15
Escherichia_coli_K12
Pseudomonas_aeruginosa_PAO1
Consensus
FAA.GKAELTGN.KLAKDFKQYALRNI.LDASFSDPSN.IDSAKFSAQGQLALDQTFEFDGRVNRK.NALTFSVKQLRAL

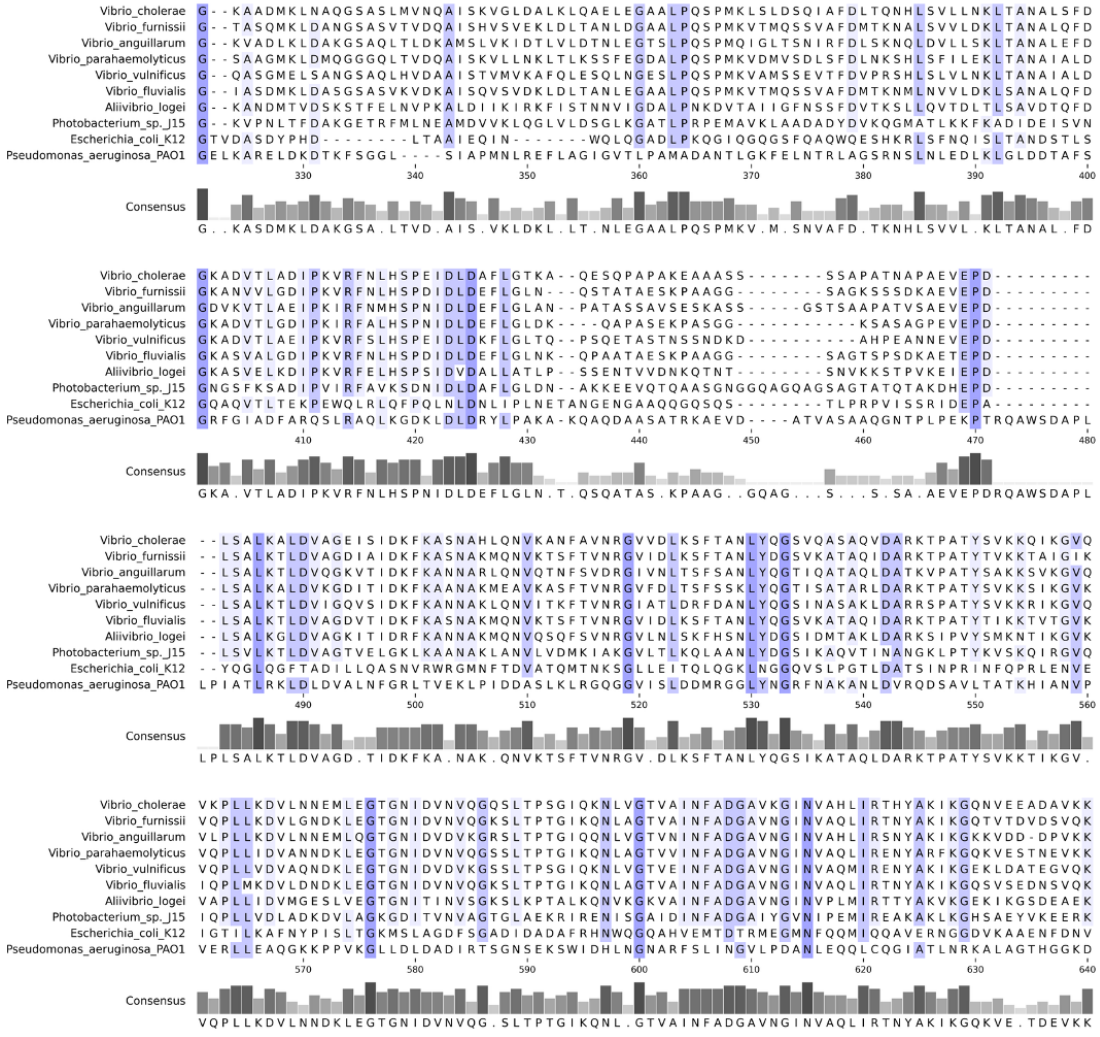
Vibrio_cholerae
Vibrio_furnissii
Vibrio_anguillarum
Vibrio_parahaemolyticus
Vibrio_vulnificus
Vibrio_fluvialis
Aliivibrio_logei
Photobacterium_sp._J15
Escherichia_coli_K12
Pseudomonas_aeruginosa_PAO1
Consensus

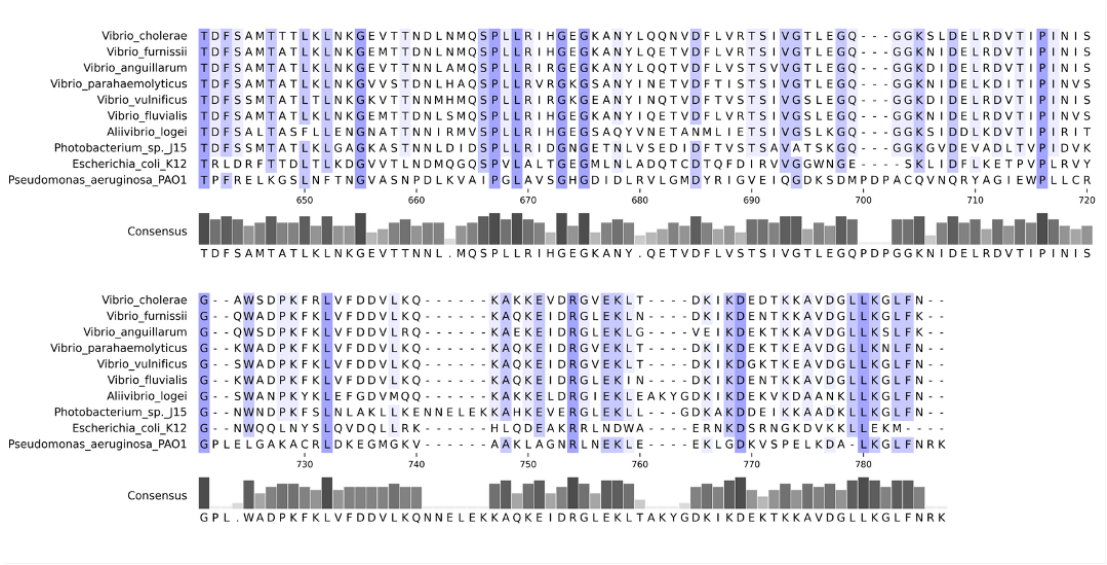
Vibrio_cholerae
Vibrio_furnissii
Vibrio_anguillarum
Vibrio_parahaemolyticus
Vibrio_vulnificus
Vibrio_fluvialis
Aliivibrio_logei
Photobacterium_sp._J15
Escherichia_coli_K12
Pseudomonas_aeruginosa_PAO1
650
660
670
680
690
700
710
720
Consensus
TDFSAMTATLKLNKGEVTTNNL.MQSPLLRIHGEGKANY.QETVDFLVSTSIVGTLEGQPDPGGKNIDELRDVTIPINIS
730
740
750
760
770
780
GPL.WADPKFKLVFDDVLKQNNELEKKAQKEIDRGLEKLTAKYGDKIKDEKTKKAVDGLLKGLFNRK

2.3.7. Previously uncharacterized genes

Our screen also identified previously uncharacterized genes in *V. cholerae*, including VCA0714, VCA0802, and VC1500. VCA0714 encodes DgkA, an enzyme that catalyzes the ATP-dependent phosphorylation of 1,2-diacylglycerol (DAG) to phosphatidic acid, a precursor for glycerophospholipid (GPL) synthesis and a phospho-form donor that modifies several surface structures. For instance, in *E. coli*, the phosphoethanolamine (pEtN) EptA modifies the lipid A component of lipopolysaccharide using phosphatidylethanolamine (PE) as the phospho-donor. EptA adds phosphoethanolamine to lipid A (19), conferring polymyxin B resistance and producing a DAG by-product in the process (20). DgkA recycles this DAG into glycerophospholipid synthesis, preventing dangerous DAG buildup and restoring phosphatidylethanolamine (PE) levels (30). Sequence and phylogenetic analyses place VCA0802 in the phosphoethanolamine to Kdo (PetK) family of LPS phosphoethanolamine transferases, where it is predicted that VCA0802 will add phosphoethanolamine (pEtN) to the single Kdo residue of the inner core of LPS (31).

VC1500 is predicted to encode an uncharacterized paraquat-inducible protein A (PqiA) and is found in an operon with VC1501, which encodes PqiB. Paraquat generates superoxide radicals, and the *pqiAB* genes were initially identified as oxidative stress-inducible and were shown to function in a transport pathway related to the Mla pathway, which maintains this asymmetry by removing phospholipids from the outer leaflet (32). VC1500 is predicted to contribute to outer membrane lipid homeostasis by maintaining lipid asymmetry (21, 22).

Transposon insertions in VCA0714, VCA0802, and VC1500 resulted in significant fitness defects (Figure 2.8A), with fitness scores of -1.90, -1.51, and -1.39, respectively (Table 2.3). In the in vitro competitive index assay of the following mutants, ΔVCA0714, ΔVCA0802, and ΔVC1500 were outcompeted by wild type after 24 hours of competition in the presence of polymyxin B (Figure 2.8B), confirming the fitness defects observed in the Bar-seq analysis.

Expression of VCA0714, VCA0802, or VC1500 from the pMMB67EH plasmid under the control of the inducible Ptac promoter complemented the corresponding mutant phenotypes and restored fitness (Figure 2.8C). In the MIC assay, the average MIC values were 13 μg/ml for ΔVCA0714, 11 μg/ml for ΔVCA0802, and 32 μg/ml for ΔVC1500, as compared to 43 μg/ml for the wild type (Figure 2.8D), indicating that deletion of VCA0714 and VCA0802 reduced polymyxin B resistance, whereas deletion of VC1500 had little effect on resistance under the conditions tested. Growth of the ΔVCA0714, ΔVCA0802, and ΔVC1500 mutants was unaffected in the presence of polymyxin B and was comparable to that of the wild type (Figure 2.8E). Collectively, these results suggest that VCA0714 and VCA0802 impact CAMP fitness, likely by facilitating LPS lipid A/Kdo modification and by affecting outer membrane lipid homeostasis.

We explored VCA0802, VCA0714, and VC1500 in *V. cholerae*, since these genes have not been studied in *V. cholerae*. We first asked how conserved these proteins are and whether we could identify orthologs in other bacteria. The closest ortholog of VCA0802 was identified in the same-genus relatives: *Vibrio anguillarum*, *Vibrio parahaemolyticus, Vibrio Vulnificus*, and *Vibrio diazotrophicus*. More distantly related orthologs in *Allivibrio logei* and *Pseudomonas aeruginosa, Mannheimia haemolytica*, and *Achromobacter insolitus* show protein conservation across evolutionary distances (Figure 2.9). The closest ortholog for VCA0714 is identified in the same-genus relatives: V*ibrio anguillarum, Vibrio diazotrophicus, Vibrio parahaemolyticus*, and *Vibrio vulnificus*. Distantly related orthologs in *Escherichia coli*, *Psychromonas sp*, *Grimontia celer*, and *Allivibrio wodanis* show protein conservation across evolutionary distance (Figure 2.10). The closest orthologs for VC1500 are the same-genus relatives: *Vibrio anguillarum, Vibrio fluviallis, Vibrio parahaemolyticus*, and *Vibrio vulnificus*. Distantly related orthologs in *Escherichia coli, Pseudomonas sp*, *Photobacterium aquae* and *Allivibrio wodanis* (Figure 2.11).

Figure 2.8. Uncharacterized genes are important for polymyxin B response.
A) Volcano plot displays genes contributing to fitness differences in the *V. cholerae* genome. The t-like test statistic is plotted on the y-axis, and the log of the fold-change (FC) (base 2) is plotted on the x-axis. Each point represents a mutant with a unique barcode. Grey lines indicate fitness cutoffs: a $\log_2$ fold-change greater than 1 (vertical lines) and a t-like test statistic greater than 3 (horizontal line). A $\log_2$ fold-change less than 1 indicates decreased fitness in the mutant compared to WT, and a log2 fold-change greater than 1 indicates increased fitness in the mutant compared to WT. Orange color indicates the mutants' uncharacterized proteins: VCA0802, VCA0714, and VC1500. B) A plot of relative fitness measured by in vitro competition of deletion mutants against the WT strain competed for 24hours. Competitive index (CI) values are plotted on a log10 scale. Means from ≥ 3 independent biological replicates were compared to WT by one-way ANOVA followed by Dunnett's multiple comparison test. Statistical comparisons were performed on log10(CI) values. Mean differences with an adjusted *P* value of ≤ 0.01 were deemed significant. *, $P \leq 0.01$; **, $P \leq 0.001$; ***, $P \leq 0.0001$; ns, not significant. Strains for which no colonies were recovered at the detection limit are indicated as ND (not detected) and were excluded from statistical comparisons. C) A plot of relative fitness measured by in vitro competition of WT with gene of interest, complemented strain, mutant with empty vector against the WT strain; WT with empty vector; competed for 24 hours. Competitive index (CI) values are plotted on a log10 scale. Means from ≥ 1 independent biological replicate were compared to WT by one-way ANOVA followed by Dunnett's multiple comparison test. Statistical comparisons were performed on log10(CI) values. Mean differences with an adjusted *P* value of ≤ 0.01 were deemed significant. *, $P \leq 0.01$; **, $P \leq 0.001$; ***, $P \leq 0.0001$; ns, not significant. Strains for which no colonies were recovered at the detection limit are indicated as ND (not detected) and were excluded from statistical comparisons. D) Bar graph of polymyxin B resistance quantification of MIC for ΔVCA0802, ΔVCA0714 and ΔVC1500 mutants. Statistical analysis, n=4 biological replicates, one-way ANOVA to compare means of mutants to WT followed by Dunnett's multiple comparison test, *$p < 0.016$ and ****$p < 0.0001$. E) Growth curves of mutants compared to WT in the presence and absence of polymyxin B. Black lines refer to WT and the orange line represents the respective mutant; solid lines represent growth in LB and dashed lines represent growth in the presence of polymyxin B, with n=3 biological replicates.

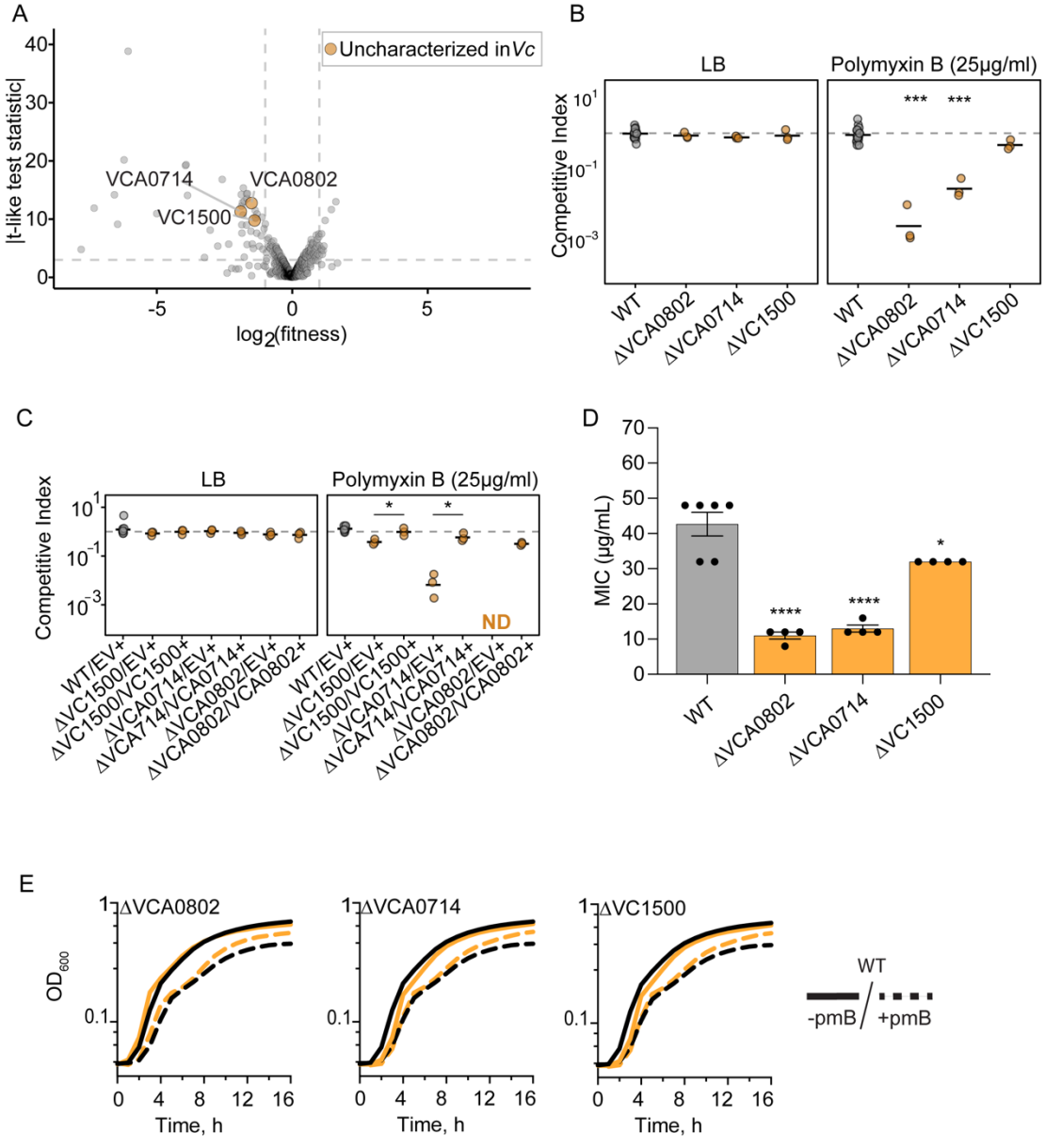
A
Uncharacterized in Vc
|t-like test statistic|
log2(fitness)
VCA0714
VCA0802
VC1500
B
LB
Polymyxin B (25µg/ml)
Competitive Index
***
***
WT
ΔVCA0802
ΔVCA0714
ΔVC1500
C
LB
Polymyxin B (25µg/ml)
Competitive Index
*
*
ND
WT/EV+
ΔVC1500/EV+
ΔVC1500/VC1500+
ΔVCA0714/EV+
ΔVCA714/VCA0714+
ΔVCA0802/EV+
ΔVCA0802/VCA0802+
D
MIC (µg/mL)
****
****
*
WT
ΔVCA0802
ΔVCA0714
ΔVC1500
E
ΔVCA0802
ΔVCA0714
ΔVC1500
OD600
Time, h
WT
-pmB
+pmB

Figure 2.9. Alignment of VCA0802 and representative orthologs
VCA0802 orthologs were identified using the EggNOG orthology database to span the range of taxonomic distances from *Vibrio cholerae* O1 biovar El Tor str. A1552, prioritizing sequences with 35-85% identity to the query within each taxonomic group and excluding fragmentary sequences (<50% of query length). Same-genus relatives: *Vibrio anguillarum*, *Vibrio parahaemolyticus*, *Vibrio Vulnificus*, *Vibrio diazotrophicus*, *Allivibrio logei, and Pseudomonas aeruginosa.* Distantly related orthologs in *Mannheimia haemolytica*, and *Achromobacter insolitus* show protein conservation across evolutionary distance. Sequences were aligned using MAFFT v7.526 (L-INS-i) and visualized with pyMSAviz v. 5.0; no trimming was performed**.**

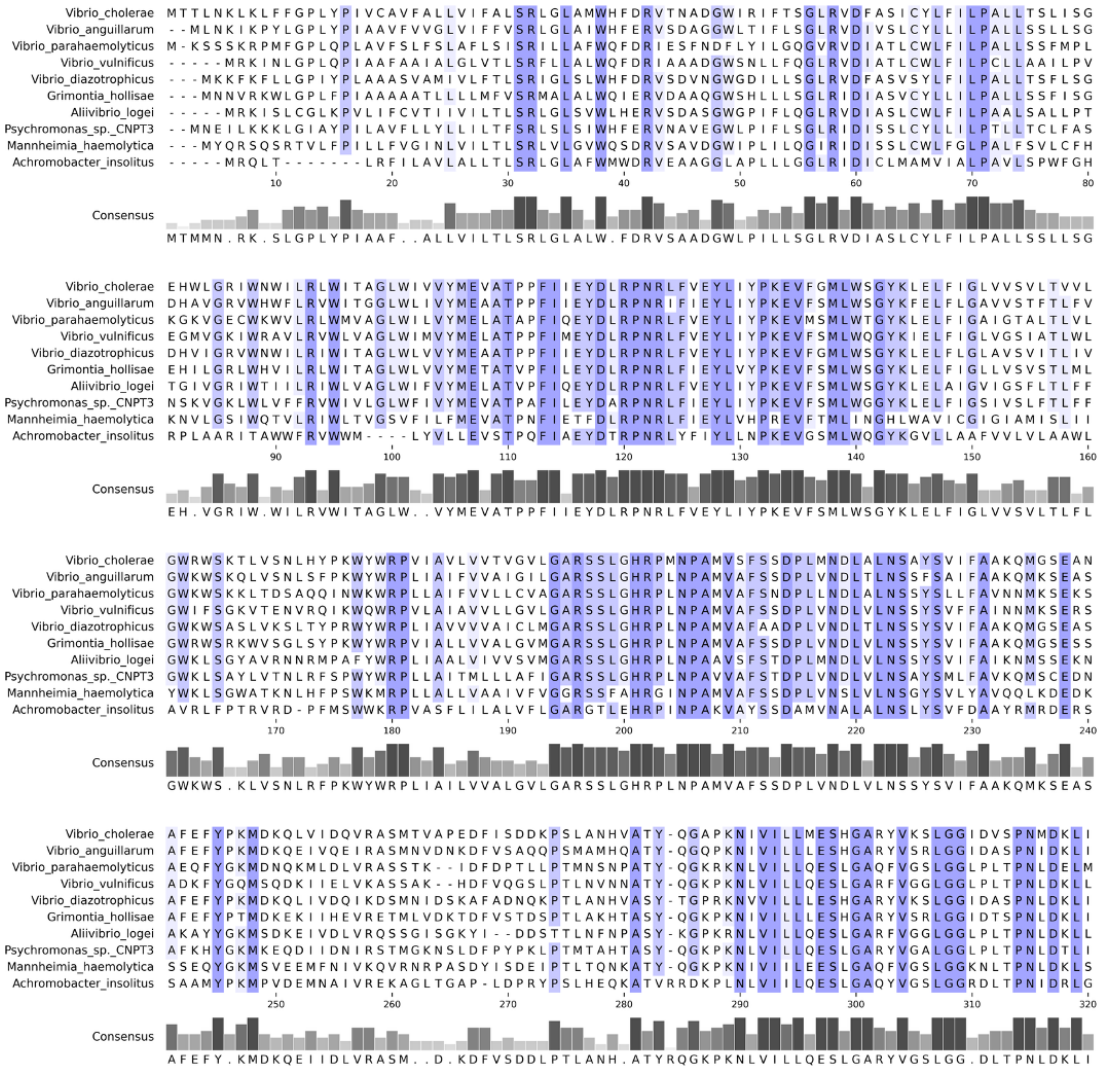
Vibrio_cholerae
Vibrio_anguillarum
Vibrio_parahaemolyticus
Vibrio_vulnificus
Vibrio_diazotrophicus
Grimontia_hollisae
Aliivibrio_logei
Psychromonas_sp._CNPT3
Mannheimia_haemolytica
Achromobacter_insolitus
Consensus
MTMMN.RK.SLGPLYPIAAF..ALLVILTLSRLGLALW.FDRVSAADGWLPILLSGLRVDIASLCYLFILPALLSSLLSG
EH.VGRIW.WILRVWITAGLW..VYMEVATPPFIIEYDLRPNRLFVEYLIYPKEVFSMLWSGYKLELFIGLVVSVLTLFL
AFEFY.KMDKQEIIDLVRASM..D.KDFVSDDLPTLANH.ATYRQGKPKNLVILLQESLGARYVGSLGG.DLTPNLDKLI

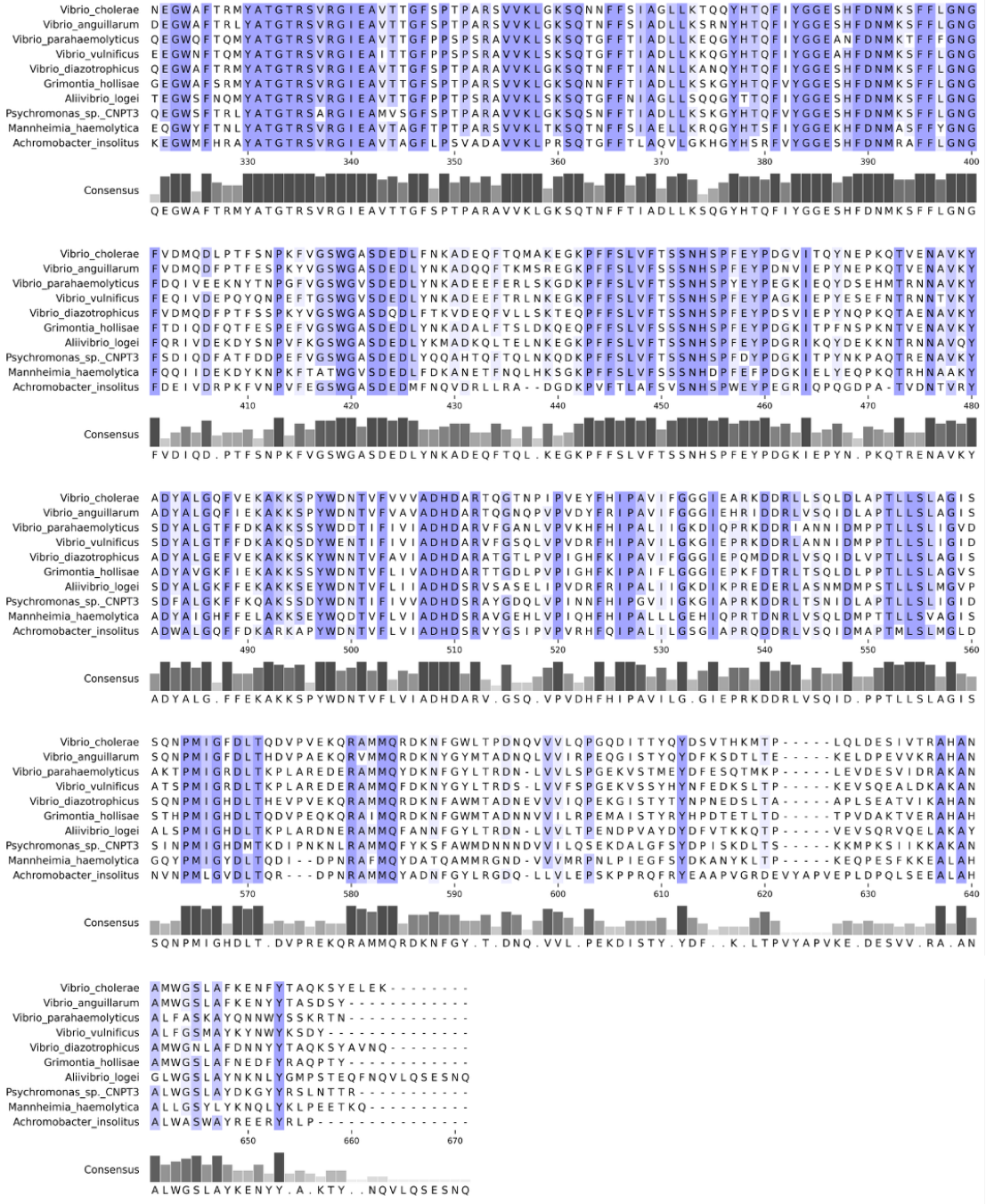
Vibrio_cholerae
Vibrio_anguillarum
Vibrio_parahaemolyticus
Vibrio_vulnificus
Vibrio_diazotrophicus
Grimontia_hollisae
Aliivibrio_logei
Psychromonas_sp._CNPT3
Mannheimia_haemolytica
Achromobacter_insolitus
Consensus

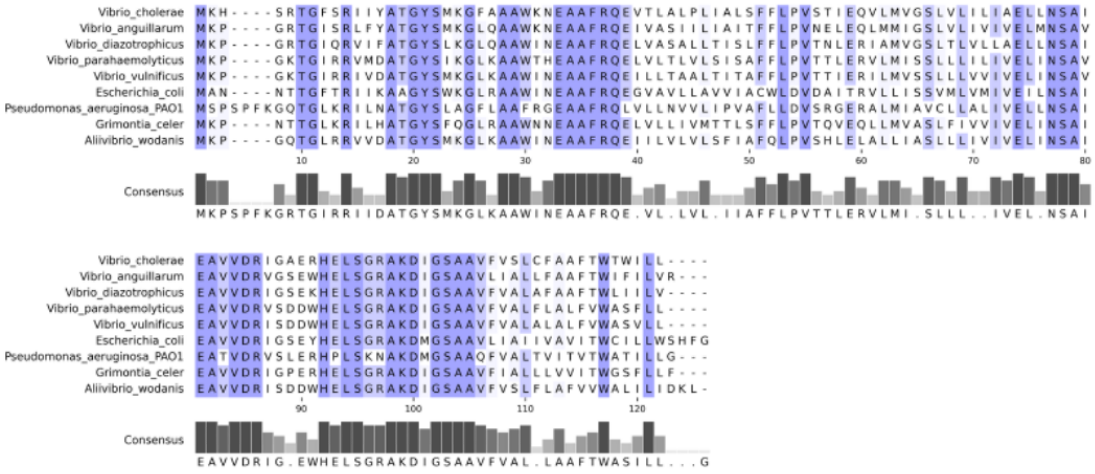

Figure 2.10. Alignment of VCA0714 representative orthologs
VCA0714 orthologs were identified using the EggNOG orthology database to span the range of taxonomic distances from *Vibrio cholerae* O1 biovar El Tor str. A1552, prioritizing sequences with 35-85% identity to the query within each taxonomic group and excluding fragmentary sequences (<50% of query length). Same genus relatives: *Vibrio anguillarum*, *Vibrio diazotrophicus, Vibrio parahaemolyticus*, *Vibrio vulnificus*. Distantly related orthologs in *Escherichia coli*, *Psychromonas sp*, *Grimontia celer*, and *Allivibrio wodanis* show protein conservation across evolutionary distance. Sequences were aligned using MAFFT v7.526 (L-INS-i) and visualized with pyMSAviz v5.0; no trimming was performed.

Figure 2.11. Alignment of VC1500 representative orthologs
VC1500 orthologs were identified using the EggNOG orthology database to span the range of taxonomic distances from *Vibrio cholerae* O1 biovar El Tor str. A1552, prioritizing sequences with 35-85% identity to the query within each taxonomic group and excluding fragmentary sequences (<50% of query length). Same genus relatives: *Vibrio anguillarum, Vibrio fluviallis, Vibrio parahaemolyticus*, *Vibrio vulnificus*. Distantly related orthologs in *Escherichia coli, Pseudomonas sp*, *Photobacterium aquae,* and *Allivibrio wodanis*. Sequences were aligned using MAFFT v7.526 (L-INS-i) and visualized with pyMSAviz v5.0; no trimming was performed.

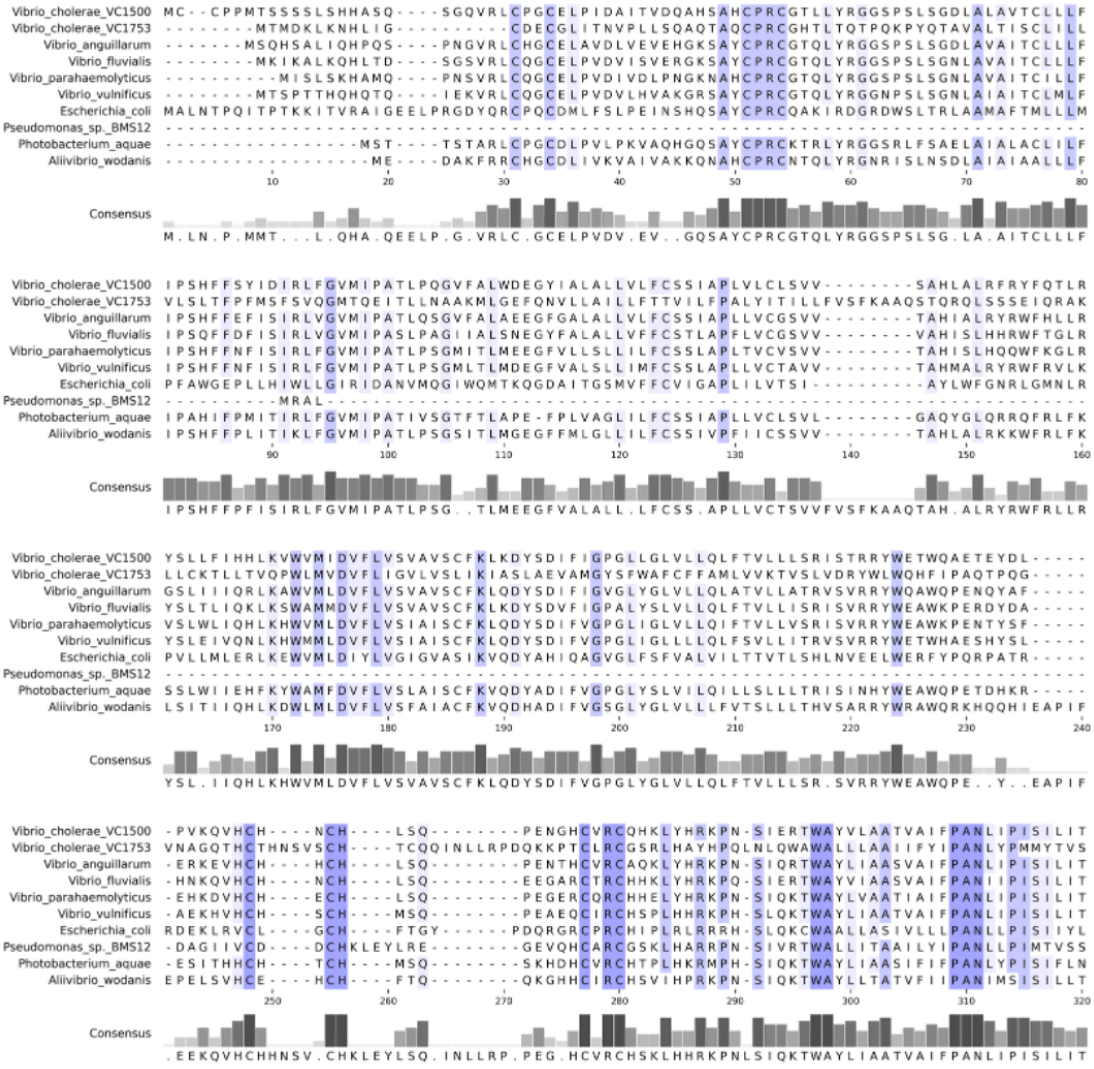
Vibrio_cholerae_VC1500
Vibrio_cholerae_VC1753
Vibrio_anguillarum
Vibrio_fluvialis
Vibrio_parahaemolyticus
Vibrio_vulnificus
Escherichia_coli
Pseudomonas_sp._BMS12
Photobacterium_aquae
Aliivibrio_wodanis
Consensus

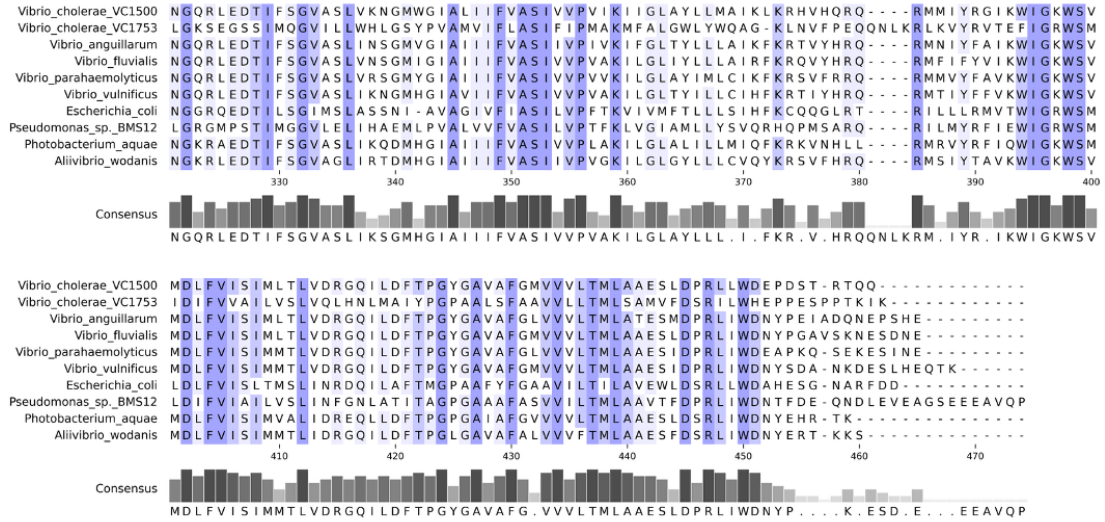
Vibrio_cholerae_VC1500
Vibrio_cholerae_VC1753
Vibrio_anguillarum
Vibrio_fluvialis
Vibrio_parahaemolyticus
Vibrio_vulnificus
Escherichia_coli
Pseudomonas_sp._BMS12
Photobacterium_aquae
Aliivibrio_wodanis
330
340
350
360
370
380
390
400
Consensus
NGQRLEDTIFSGVASLIKSGMHGIAIIIFVASIVVPVAKILGLAYLLL.I.FKR.V.HRQQNLKRM.IYR.IKWIGKWSV
410
420
430
440
450
460
470
Consensus
MDLFVISIMMTLVDRGQILDFTPGYGAVAFG.VVVLTMLAAESLDPRLIWDNYP....K.ESD.E...EEAVQP

2.3.8. Mutants identified in BarSeq analysis contribute to cationic antimicrobial peptide LL-37

To determine whether the genes identified in BarSeq confer resistance to the broad-spectrum cationic antimicrobial peptide LL-37, we measured LL-37 MICs starting at 250 µg/ml and diluted in 2-fold serial dilutions, with each well containing 100 µL of cells. MICs were 31.2 µg/ml for Δ*carR,* 125 µg/ml for ΔVC1039, ΔVCA0802, and ΔVCA0714, compared to 250 µg/ml for wild type (Figure 2.12). These results support the idea that the absence of these genes decreases resistance to LL-37 and contributes to general CAMP resistance.

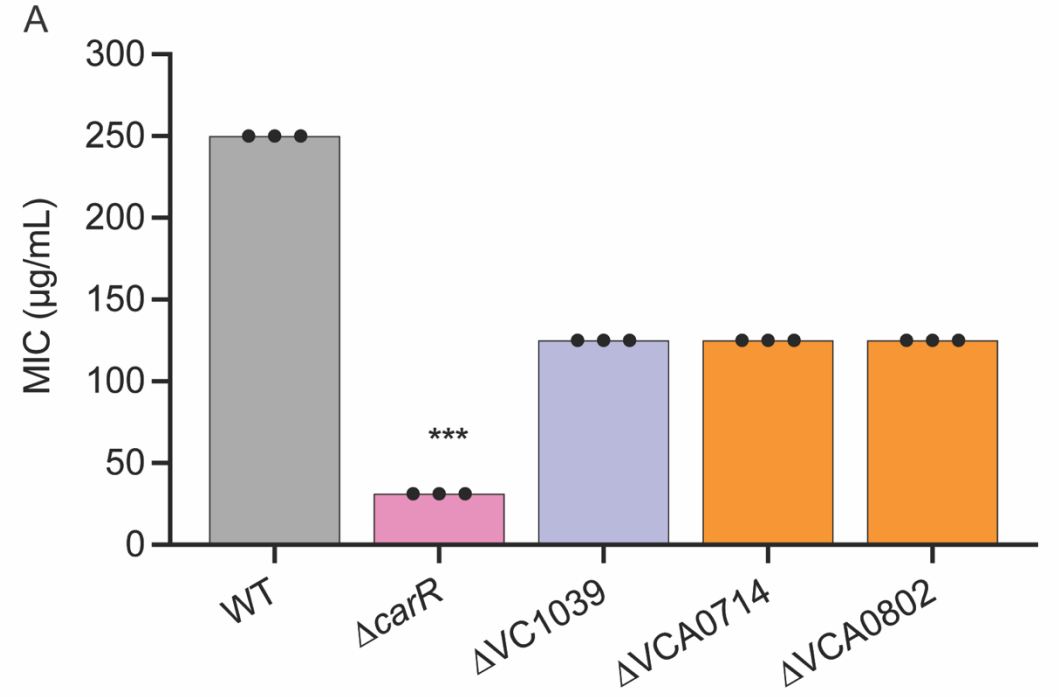

Figure 2.12. Genes contributing to LL-37 resistance
Bar graph of LL-37 resistance quantification of the MIC values for the Δ*carR*, ΔVC1039, ΔVCA0714, and ΔVCA0802 mutants. Statistical analysis of three biological replicates (n=3): one-way ANOVA to compare means of mutants to WT, followed by Dunnett's multiple comparison test, ***$p < 0.0001$.

2.3.9. RfbD and GalU contribute to envelope stress sensing

To test whether genes identified as contributing to polymyxin B fitness are also involved in general envelope stress sensing, we selected genes that decreased fitness and polymyxin B resistance. We first determined general envelope stress sensing by measuring outer membrane homeostasis. We analyzed sensitivity to bile and SDS-EDTA. As controls, we used *an ompU* mutant known to be sensitive to envelope stress(23) and an *mla* operon mutant with a predicted compromised outer membrane lipid asymmetry that is important for membrane integrity (21). Mutations in *ompU* and the *mla* operon resulted in increased sensitivity to outer membrane disruptors, Ox Bile, and treatments that disrupt lipid bilayer packing (24), while SDS-EDTA treatment chelates magnesium (Mg^{2+}) and calcium (Ca^{2+}) that stabilize LPS structure (25). If the genes we identified in the Barseq that contribute to fitness differences in the presence of polymyxin B also cause general outer membrane permeability defects, we expect them to show increased sensitivity to these treatments compared to wild type, comparable to Δ*ompU* and Δ*mla* mutants. As expected, the *ompU* and *mlaA* mutants showed sensitivity to Ox bile and SDS-EDTA, with impaired growth and decreased OD compared to wild type. We tested a subset of genes that showed fitness differences in the presence of polymyxin B, including LPS mutants Δ*galU* and Δ*rfbD, which* showed decreased growth compared to wild type in the presence of 0.01% Ox Bile (Figure 2.13). and in the presence of 0.01% SDS + 0.1mM EDTA (Figure 2.14). No other mutants from the Barseq showed growth defects in the presence of 0.01% Ox Bile (Figure 2.13) and in the presence of 0.01% SDS + 0.1mM EDTA (Figure 2.14). Further exploration of general envelope stress is needed, but these data suggest that *rfbD* and *galU* mutants affect general envelope stress, indicating that O-antigen and core-oligosaccharide genes are important for outer membrane permeability and homeostasis.

Figure 2.13. Lipopolysaccharide genes contribute to fitness differences in the presence of polymyxin B and to envelope permeability

Growth curves of WT (black) and mutant (color), grown in LB (solid line) and in the presence of 0.01% ox-bile (dashed line) at 37˚C. CarR regulon members in pink (A), LPS mutants in green (C), VC1039 and uncharacterized in *V. cholerae* in purple and orange, respectively (D), envelope stress controls the *mla* operon in blue, and Δ*ompU* in maroon.

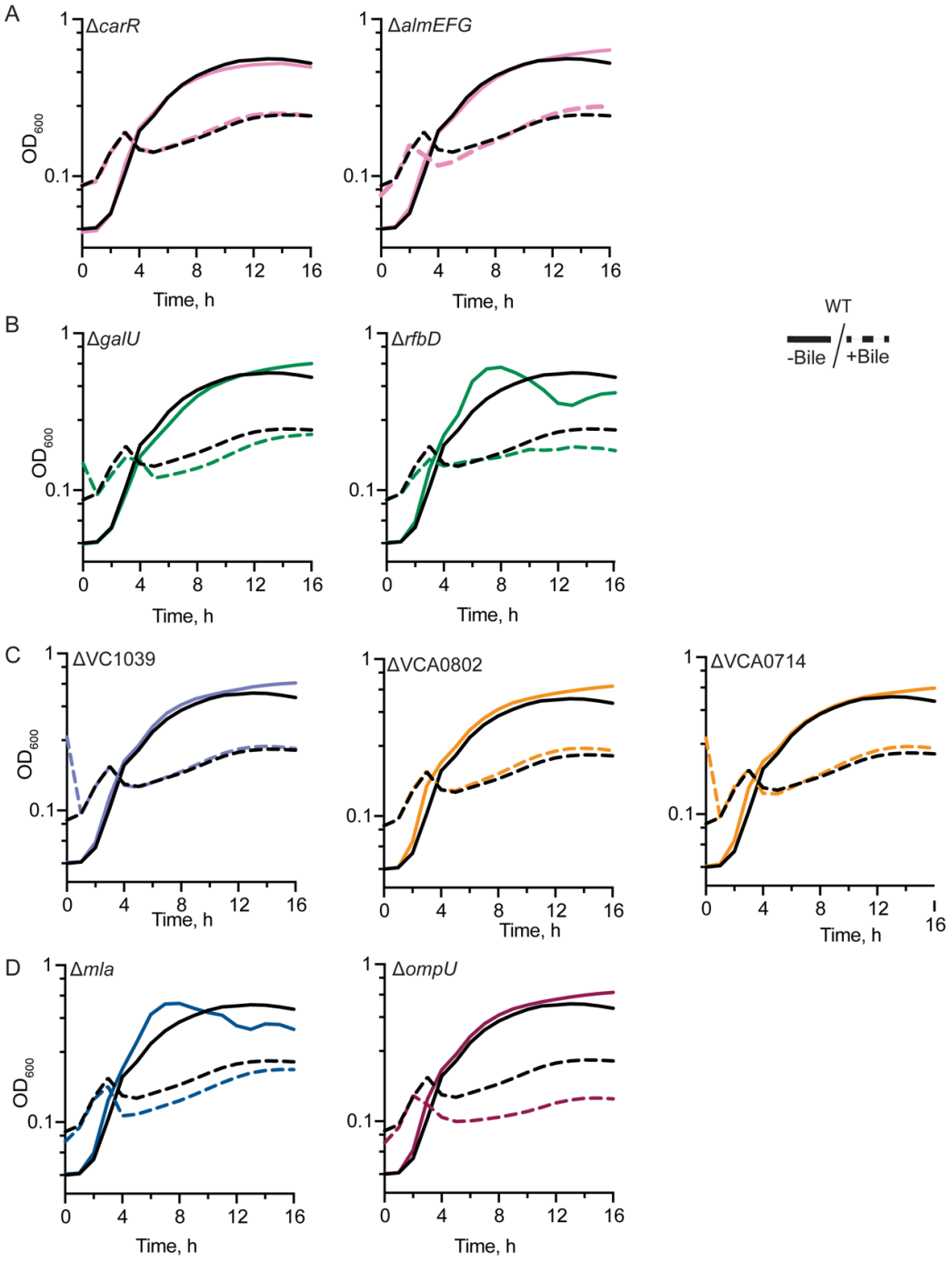
A
ΔcarR
ΔalmEFG
B
ΔgalU
ΔrfbD
WT
-Bile
+Bile
C
ΔVC1039
ΔVCA0802
ΔVCA0714
D
Δmla
ΔompU
OD600
Time, h
1
0.1
0
4
8
12
16

Figure 2.14. Lipopolysaccharide genes contribute to fitness differences and to envelope homeostasis in the presence of SDS

Growth curves of WT (black) and mutant (color), grown in LB (solid line) and in the presence of SDS+EDTA (dashed line) at 37˚C. CarR regulon members in pink (A), LPS mutants in green (C), VC1039 and uncharacterized in *V. cholerae* in purple and orange, respectively (D), envelope stress controls the *mla* operon in blue, and Δ*ompU* in maroon.

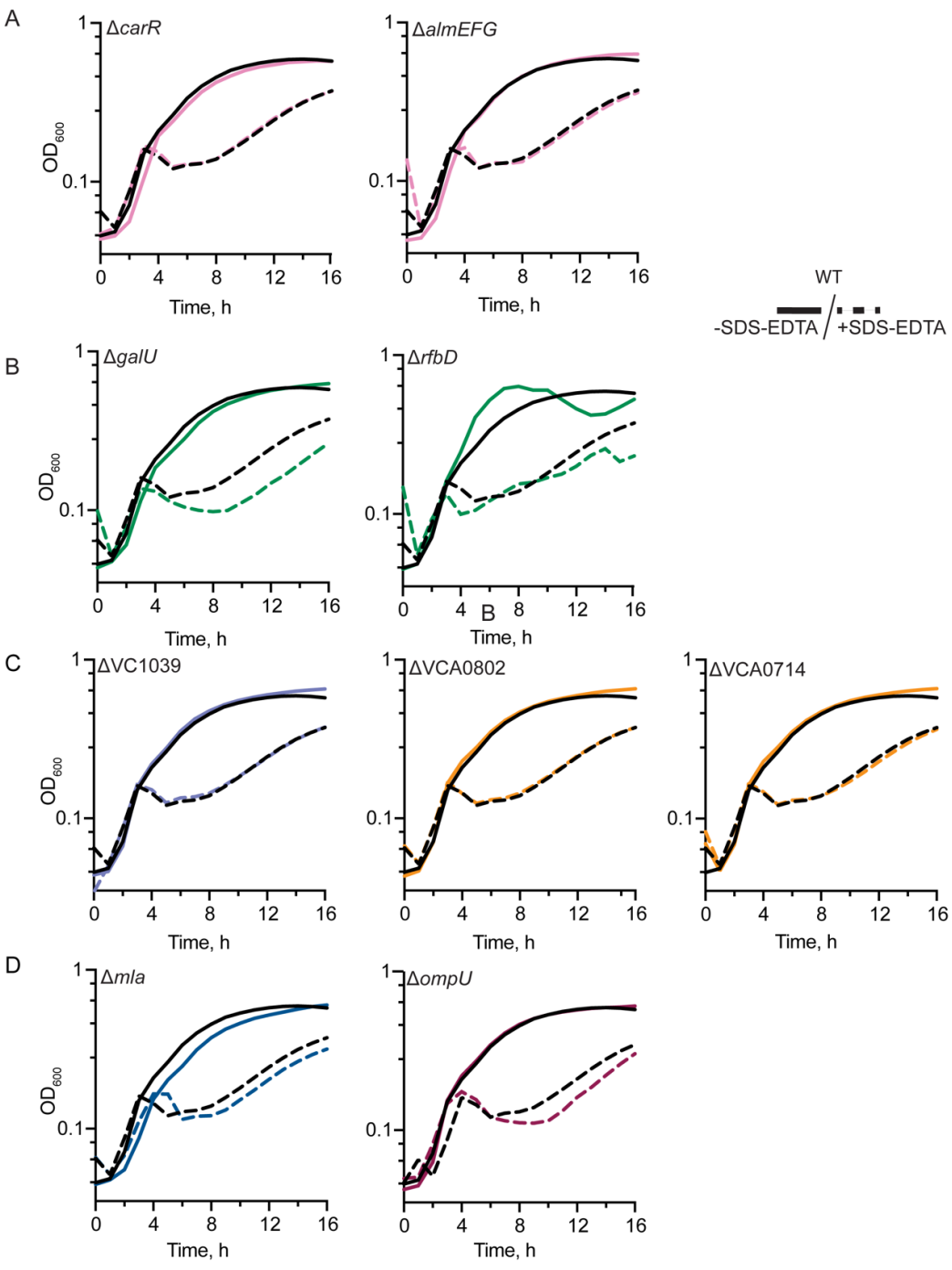
A
ΔcarR
ΔalmEFG
WT
-SDS-EDTA
+SDS-EDTA
B
ΔgalU
ΔrfbD
C
ΔVC1039
ΔVCA0802
ΔVCA0714
D
Δmla
ΔompU
OD600
Time, h
0.1
1
0
4
8
12
16

Table 2.5 Bacterial strains and plasmids used in this work

Strain or plasmid	Description	Source
E. coli		
DH5α-λ*pir*	end*A1 hsdR17 gln*V44 (-supE44) thi-1 *recA gyrA*96 *rel*A1 ϕ80*dlac*Δ*(lacZ)M15* Δ*(lacZYA-argF)U169 zdg-232::Tn10 uidA::pir+*	47
S17-1λ*pir*	Tp^r Sm^r *rec Athi pro* r_{k-} m_{k+} RP4::2-Tc::MuKm Tn7 λ*pir*	48
V. cholerae		
FY_Vc_1	*Vibrio cholerae* O1 El Tor A1552, wild type, Rif^r	49
FY_Vc_628	Δ*lacZ,* Rif^r	50
FY_Vc_237	FY_Vc_1 Tn7*::gfp* Rif^r, Gm^r	51
FY_Vc_3274	Δ*carS* (VC1319), Rif^r	13
FY_Vc_3275	Δ*carS* (VC1319) Tn7*::gfp* Rif^r	13
FY_Vc_3282	Δ*carR* (VC1320), Rif^r	13
FY_Vc_3283	Δ*carR* (VC1320) Tn7*::gfp* Rif^r	13
FY_Vc_20788	$carR^{D55E}$,Rif	This study
FY_Vc_20789	$carR^{D55A}$,Rif^r	This study
FY_Vc_20790	$carS^{H222A}$,Rif^r	This study
FY_Vc_20791	$carS^{D223A}$,Rif^r	This study

Strain or plasmid	Description	Source
FY_Vc_20792	*carS*^{T226A}, Rif^{r}	This study
FY_Vc_4091	Δ*almG* (VC1576), Rif^{r}	8
FY_Vc_4094	Δ*almF* (VC1577), Rif^{r}	8
FY_Vc_4097	Δ*almE* (VC1578), Rif^{r}	8
FY_Vc_13625	Δ*ompV* (VC1318), Rif^{r}	Yildiz lab collection
FY_Vc_10972	Δ*rfbD* (VC0243) Rif^{r}	55
FY_Vc_20697	Δ*galU* (VC0395), Rif^{r}	This study
FY_Vc_20699	ΔVCA0714, Rif^{r}	This study
FY_Vc_20700	ΔVC1500, Rif^{r}	This study
FY_Vc_20701	ΔVCA0802, Rif^{r}	This study
FY_Vc_20703	ΔVC0851, Rif^{r}	This study
FY_Vc_20704	ΔVC1039, Rif^{r}	This study
FY_Vc_20705	ΔVC2156, Rif^{r}	This study
FY_Vc_20708	Δ*wbeV* (VC0260), Rif^{r}	This study
FY_Vc_20793	WT+pMMB67EH-VC0851, Rif^{r,} Amp^{r}	This study
FY_Vc_20794	ΔVC0851+pMMB67EH-VC0851, Rif^{r,} Amp^{r}	This study
FY_Vc_20795	ΔVC0851 +pMMB67EH-empty vector (EV), Rif^{r,} Amp^{r}	This study

Strain or plasmid	Description	Source
FY_Vc_20796	WT+pMMB67EH-*galU*, Rif^r, Amp^r	This study
FY_Vc_20797	Δ*galU* +pMMB67EH-*galU*, Rif^r, Amp^r	This study
FY_Vc_20798	Δ*galU*+pMMB67EH-empty vector (EV), Rif^r, Amp^r	This study
FY_Vc_20799	WT+pMMB67EH-*wbeV*, Rif^r, Amp^r	This study
FY_Vc_20800	Δ*wbeV* +pMMB67EH-*wbeV*, Rif^r, Amp^r	This study
FY_Vc_20801	Δ*wbeV*+pMMB67EH-empty vector (EV), Rif^r, Amp^r	This study
FY_Vc_20802	WT+pMMB67EH-*rfbD*, Rif^r, Amp^r	This study
FY_Vc_20803	Δ*rfbD* +pMMB67EH-*rfbD*, Rif^r, Amp^r	This study
FY_Vc_20804	Δ*rfbD*+pMMB67EH-empty vector (EV), Rif^r, Amp^r	This study
FY_Vc_20805	WT+pMMB67EH-VC2156, Rif^r, Amp^r	This study
FY_Vc_20806	ΔVC2156+pMMB67EH-VC2156, Rif^r, Amp^r	This study
FY_Vc_20807	ΔVC2156+pMMB67EH-empty vector (EV), Rif^r, Amp^r	This study
FY_Vc_20808	WT+pMMB67EH-VC1039 Rif^r, Amp^r	This study
FY_Vc_20809	ΔVC1039+pMMB67EH-VC1039, Rif^r, Amp^r	This study
FY_Vc_20810	ΔVC1039 +pMMB67EH-empty vector (EV), Rif^r, Amp^r	This study

Strain or plasmid	Description	Source
FY_Vc_20813	WT+pMMB67EH-VCA0714, Rif^r, Amp^r	This study
FY_Vc_20814	ΔVCA0714+pMMB67EH-VCA0714, Rif^r, Amp^r	This study
FY_Vc_20815	ΔVCA0714+pMMB67EH-empty vector (EV), Rif^r, Amp^r	This study
Plasmids		
pFY_23	pGP704 derivative; mob-ori, sacB, Amp^r	G. Schoolnik
pFY_117	pGP704::mTn7-*gfp*, Gm^r, Amp^r	52
pFY_118	oriR6K helper plasmid, *mob-oriT,* provides the Tn7 transposition function in *trans,* Amp^r	52
pFY_8386	pGP704sacB-*carR*^{D55A}	This study
pFY_8394	pGP704sacB-*carR*^{D55E}	This study
pFY_8396	pGP704sacB-*carS*^{H222A}	This study
pFY_8388	pGP704sacB-*carS*^{D223A}	This study
pFY_8387	pGP704sacB-*carS*^{T226A}	This study
pFY_8397	pGP704sacB-*carRS* (VC1319-20)	This study
pFY_8398	pGP704sacB-*dbfRS* (VC1638-39)	This study
pFY_4769	pGP704sacB-*galU* (VC0395)	56
pFY_4942	pGP704sacB-*webV* (VC0260)	55

Strain or plasmid	Description	Source
pFY_8391	pGP704sacB-VCA0802	This study
pFY_8389	pGP704sacB-VC1500	This study
pFY_8390	pGP704sacB-VCA0714	This study
pFY_8401	pGP704sacB-VC2156	This study
pFY_8402	pGP704sacB-VC0851	This study
pFY_8403	pGP704sacB-VC1039	This study
pFY_1303 (pMMB67EH)	Expression vector harboring *lacI* and P_{tac} promoter, Amp^r	Yildiz lab collection
pFY_8423	pMMB67EH-VCA0714	This study
pFY_8424	pMMB67EH-VC0851	This study
pFY_8425	pMMB67EH-VC2156	This study
pFY_8426	pMMB67EH-VC1039	This study
pFY_8427	pMMB67EH-*galU* (VC0395)	This study
pFY_8428	pMMB67EH-*wbeV* (VC0260)	This study
pFY_8429	pMMB67EH-*rfbD* (VC0243)	This study
pFY_8432	pMMB67EH-VC1500	This study
pFY_8433	pMMB67EH-VCA0802	This study
pFY_691	*luxCDABE*-based promoter fusion vector, Cm^r	52

Strain or plasmid	Description	Source
pFY_3406	pBBR*lux vpsL* promoter, Cm^r (-607, +158)	54

2.4 **Discussion**

In this study, we used a multi-omics approach to identify genetic determinants associated with polymyxin B sub-MIC sensitivity. RNA-seq and Barseq screens identified known determinants of polymyxin B response (*carR, carS*, *almE*, *almF*, *almG*) and previously uncharacterized genes: VC1039, VC0851, VC2156, VCA0802, VCA0714, and VC1500. Deletions of these genes significantly decreased the MIC for polymyxin B, a cationic antimicrobial peptide. We wanted to determine whether these genes are important for resistance to the cationic antimicrobial peptide produced by mammals, LL-37 (26, 27). We determined the MICs of these mutants relative to the wild type in the presence of LL-37. We tested only the previously uncharacterized genes identified in the polymyxin B Barseq; we found that these genes are also required for resistance to LL-37. CAMP resistance often induces the envelope stress response; we wanted to determine whether these genes caused an envelope stress defect. We did this by growing these mutants along with envelope-defective controls: Δ*ompU* and Δ*mla* operon in the presence of membrane-disturbing compounds. We tested VC1039, VC0851, VC2156, VCA0802, VCA0714, and VC1500; none caused a general envelope defect compared with Δ*ompU* and Δ*mla* (Figures 2.13 and 2.14). In the following section, I describe each of these genes and speculate how they might contribute to polymyxin B fitness.

Lipopolysaccharide biosynthesis genes *galU, rfbD* and *wbeV*

galU and rfbD mutants exhibited reduced fitness in the presence of polymyxin B, were outcompeted by the wild type under the same conditions, and showed decreased resistance

to polymyxin B. These mutants were expected to be important for the polymyxin B response, since *galU and rfbD* are involved in the O-antigen sugar and core oligosaccharide of lipopolysaccharide (28). These lipopolysaccharide structures, *galU* and *rfbD,* are found in the outer membrane, support membrane growth, and form a protective barrier for the cell. These structures change when cationic compounds such as polymyxin B electrostatically interact with the lipid A portion of lipopolysaccharide (29). The *wbeV* mutant showed decreased fitness in Barseq but no defects in in vitro competition or polymyxin B resistance. We expected the *wbeV* mutant to be important for polymyxin B resistance and in vitro competition. The *wbeV* mutant had no growth defect, suggesting additional genes with similar functions or that *wbeV*'s role is in synthesizing the O-antigen backbone of lipopolysaccharide.

Outer membrane biogenesis genes: VC1039, VC0851, and VC2156.

The VC1039 mutant *showed* decreased fitness in the Barseq; ΔVC1039 decreased relative fitness and resistance in the presence of polymyxin B. These data suggest VC1039 is important for the polymyxin B response. VC1039 has not been studied in *V. cholera*e, but we know it contains an ASMA domain. ASMA-domain-containing proteins have a distinct N-terminal chorein domain lined with hydrophobic residues, allowing interaction with glycerophospholipids. The C-terminus contains a signature β-taco fold (27) that forms a tunnel for bulk phospholipid movement from the inner membrane to the outer membrane through the periplasm, which is important for outer membrane biogenesis observed in *E. coli* and *P. aeruginosa* (30). Sequence alignment of VC1039 across taxonomic groups shows little conservation (Figure 2.7). The absence of VC1039 could impair cells' ability to repair the outer membrane by impeding the transfer of phospholipid precursors for outer membrane biogenesis, Field (23), thereby limiting the rebuilding of outer membrane structures important for growth and barrier protection in response to polymyxin B.

VC0851 and VC2156 mutants in the Barseq resulted in decreased fitness in the presence of polymyxin B and decreased resistance to polymyxin B compared to wild type. VC0851 and VC2156 are not well studied in *V. cholerae* but are predicted to be auxiliary proteins that comprise the ß-barrel assembly machinery (BAM complex) found on the outer membrane. The BAM complex folds and inserts proteins into the outer membrane. This complex consists of five proteins: BamA, BamB, BamC, BamD, and BamE (32–34). Only *bamA* and *bamD* are essential for cell growth, whereas a Δ*bamC* decreased stabilization of the BAM complex in the presence of polymyxin B (35). BamB-E proteins are lipoproteins and are expected to anchor to the periplasmic side of the outer membrane. These data establish the relationship between fitness, measured by the Barseq, and resistance, determined by the MIC, identifying VC0851 and VC2156 as candidates important for polymyxin B response by contributing to polymyxin B resistance.

Previously uncharacterized genes in *V. cholerae* include VCA0802, VCA0714, and VC1500. While VCA0802 is uncharacterized in *V. cholerae*, a homolog found in *Vibrio vulnificus* has been shown to be downregulated in the absence of *carR* (36). In *Vibrio vulnificus* and in *Pasteurella multocida* (20), VCA0802 is predicted to modify the Kdo sugar residue found in the core-LPS. This modification pathway has been shown to be important for cationic antimicrobial peptide cathelicidin-2 (20) and has increased multidrug resistance by modifying LPS (37) in the outer membrane.

VCA0714 is a homolog of diacylglycerol kinase (*dgkA*). *dgkA* is well studied in *E. coli*. DgkA is activated when increased concentrations of diacylglycerol are sensed (36). Diacylglycerol concentrations increase when phosphoethanolamine is added to lipid A or when anionic phospholipids increase during the stationary phase as part of the stringent response. VCA0714 is predicted to add phosphate to diacylglycerol as a signal for re-introduction into the phospholipid pathway, and VCA0714 is involved in the phospholipid recycling process

(30). Removal of this recycling mechanism is important for polymyxin B exposure. In *V. vulnificus,* orthologs of VCA0802 and VCA0714 are in an operon. Given their phenotypes, further genetic analysis through double deletion of VCA0802 and VCA0714 is needed to determine whether these two genes are in the same genetic pathway in *V. cholerae* involved in the polymyxin B response. VC1500 encodes an inner membrane protein that contains a mammalian cell entry (MCE) domain (37). MCE-domain-containing proteins correct mislocalized lipids to maintain outer membrane lipid asymmetry, which has been shown to affect antibiotic resistance and outer membrane stress (58,59). The absence of VC1500 could result in an interruption of the outer membrane's ability to correct mislocalized lipids; outer membrane instability could be further exacerbated upon exposure to polymyxin B, indicating that VC1500 is important for the polymyxin B response.

Our screen also gave unexpected results. *ompV* has previously been shown to contribute positively to polymyxin resistance (18). In our experiments, the *ompV* deletion exhibited increased fitness. This can be attributed to OmpV, when present, encoding a porin with an electronegative pocket in the barrel lumen (14), acting as a port of entry for polymyxin B, or to changes in outer membrane composition when the OmpV porin is removed, as previously shown in Gram-negative *E. coli* (38). In either case, we predicted that *ompV* mutants would show reduced polymyxin B interactions with the outer membrane and thus higher fitness.

Further exploration is required to determine the response to the general cationic antimicrobial peptide, LL-37. We identified genes involved in resistance to this CAMP by measuring LL-37 MICs. MICs for *carR*, VC1039, VCA0802, and VCA0714 were lower than wild type. The *carR* mutant showed a significant decrease in LL-37 MIC, as expected, since *carR* mutants are sensitive to cationic antimicrobial peptides (18, 35, 39, 40). LL-37 has a positive charge of ($^{+}$6) compared to polymyxin B ($^{+}$5) (41–43), and this charge helps it function as a cationic antimicrobial peptide by destabilizing the outer membrane (38). Decreased MICs for selected

mutants and the Δ*carR* mutant may indicate their importance for resistance in the presence of LL-37. Additional studies comparing cell viability among the mutants would clarify the response to LL-37. This study provides new insights into the genetic determinants of *V. cholerae* cationic antimicrobial peptide response.

2.5 **Materials and methods**

2.5.1. Bacterial strains, plasmids, and growth conditions

Table 1 lists the strains and plasmids used in this study. All *V. cholerae* and *E. coli* strains were grown in Luria-Bertani (LB) medium (0.5% yeast extract, 1% tryptone, 1% NaCl, pH 7.5) at 30˚C and 37˚C, respectively, with 200 rpm shaking, unless otherwise indicated. Granulated LB agar medium included granulated agar (BD Difco, Franklin Lakes, NJ) at 1.5% (wt/vol). Antibiotics and inducers were used, when necessary, at the following concentrations: ampicillin 100μg/mL; rifampin 100μg/mL; and isopropyl β-D-1-thiogalactopyranoside (IPTG) 100μM. Unless otherwise specified, overnight cultures were prepared as follows: strains were streaked from frozen glycerol stock onto LB agar plates and grown overnight at 30˚C. 5 colonies were then inoculated into 5 mL LB medium and grown overnight at 30˚C with aeration (200 rpm).

2.5.2. Strain and plasmid construction

Plasmids were constructed using standard cloning methods for the Gibson Assembly recombinant DNA technique (New England Biolabs, Ipswich, MA). Restriction enzymes were purchased from New England Biolabs. Gene-in-frame deletions were performed using an allelic exchange of the native open reading frame (ORF) with the truncated ORF as previously described (46). Polymerase chain reactions (PCRs) were carried out with primers purchased from Integrated DNA Technologies, and sequencing of plasmid constructs was performed at the Genewiz/Azenta Life Sciences (Chelmsford, MA) company. All *V. cholerae* sequences were amplified from genomic DNA isolated from *V. cholerae* A1552 strain. For complementation constructs, the open reading frame of the gene of interest was cloned into pMMB67EH, which contains the IPTG-inducible *Ptac* system. The resulting plasmid was transformed into *E. coli* and DH5α-λ*pir* donor strain and introduced into the *V. cholerae* A1552 strain by conjugation.

2.5.3. Barseq growth conditions

The random barcoded library was generated using the Mariner vector with a DNA barcode conjugated into *V. cholerae*. Cells were collected, DNA was sheared, and Illumina adaptors were added. DNA barcode and transposon insertion site were identified by randomly barcoded transposon sequencing (47). The randomly barcoded transposon mutant library was grown in LB broth with 50µg/ml of kanamycin at 30˚C with 200 rpm shaking and diluted to an $OD_{600\ of}$ 0.5. The library was then sub cultured 1/500 in LB, with and without polymyxin B. Cells were exposed to polymyxin B for 2.5 hours over 2 passages. 2 mL of cells were pelleted for genomic DNA extraction, followed by PCR amplification of DNA barcodes for quantification. DNA barcodes were identified by Illumina sequencing using 150 paired-end reads, and 150 reverse reads were used for quantification of DNA-barcode abundance.

2.5.4. In vitro competition assays

Wild-type reference strain (*lacZ*$^+$+pMMB67EH vector) and each *lacZ*$^+$ *V. cholerae* mutant strain were used for competition. Cultures of relevant strains were grown overnight at 30 °C with shaking at 200 rpm in LB + 100 µg/mL ampicillin. Cultures were then diluted 1/10 in LB broth +100 µg/mL ampicillin (Amp) and competed at a 1:1 ratio in LB broth +100 µg/mL ampicillin (Amp), with or without 25 µg/mL polymyxin B, for 6 and 24 hours. The inoculum was plated on LB agar plates containing 5-bromor-4-chloro-3-indoyl-ß-D-galactopyranoside (x-gal), Rif, and Amp to differentiate colonies of the reference strain from mutants. In vitro competitive indices were then calculated by dividing [polymyxin B output/ polymyxin B input] by [LB output / LB input].

2.5.5. Minimum inhibitory concentration

V. cholerae liquid cultures grown overnight at 30˚C with 200 rpm shaking were diluted to OD_{600} 0.3, and 150µL were spread on 15 mL 150 × 15 mm LB agar medium plates, dried, and an E-strip of polymyxin B (Thermo Fisher) was applied.

2.5.6. Growth curves

V. cholerae strains were grown aerobically overnight at 30˚C with 200 rpm in LB. Strains were diluted 1:200 in 200 µL of medium into a single well of a 96-well plate. 96-well plates were incubated in a plate reader at 37˚C in LB with and without 25 µg/mL polymyxin B. OD_{600} measurements were taken hourly after brief shaking to stir the cells. 3 biological replicates (independent overnight cultures) and 3 technical replicates (same overnight culture in different wells) were used to compare growth between conditions using a PerkinElmer Victor3 multilabel counter (PerkinElmer, Waltham, MA).

2.5.7. LL-37 minimum inhibitory concentration

V. cholerae liquid cultures grown overnight at 30˚C with 200 rpm shaking were diluted to OD_{600} 0.3. Cells were pelleted and resuspended in 10% LB. 100µL of cells were added to 100µL of 2-fold diluted LL-37, starting with a concentration of 200µg/ml. Cells were incubated for 18 hours at 37 °C at 100 rpm. OD_{600} measurements were taken. 3 biological replicates (independent overnight cultures) and 3 technical replicates (same overnight culture in different wells) were used to compare growth using a PerkinElmer Victor3 multilabel counter (PerkinElmer, Waltham, MA).

2.5.8. Statistical analysis

Statistical performed statistical analyses using GraphPad Instat, with ANOVA as indicated.

Chapter 3 Dual Role of the CarRS two-component system in antimicrobial peptide resistance and biofilm regulation in *Vibrio cholerae*

3.1 Abstract

Bacterial environmental stress response often relies on two-component signaling (TCS) systems, which typically consist of a sensor histidine kinase (HK) and a response regulator (RR). The genome of the facultative human pathogen *Vibrio cholerae* encodes numerous HK and RR proteins, highlighting the importance of TCS in its adaptability and pathogenicity. Among these, the CarRS two-component regulatory system is critical for responding to antimicrobial peptides and conferring resistance to these compounds. Notably, CarR is one of the few regulators known to negatively regulate biofilm formation in *V. cholerae*. However, the molecular mechanisms through which the CarRS system controls biofilm formation and dispersal remain poorly understood. In this study, we investigated the impact of CarS and CarR phosphorylation states and explored the role of CarR-regulated genes in polymyxin B exposure and their essential contribution to resistance. Our findings show that CarRS phosphorylation states partially influence phenotypic outcomes and affect both antimicrobial resistance and biofilm formation. These results provide insights into the CarRS TCS system, revealing its dual role in mediating antimicrobial resistance and regulating biofilm dynamics in *V. cholerae*.

3.1 Introduction

Vibrio cholerae can exist in planktonic and biofilm forms in the aquatic and host environments. Biofilm formation occurs when a single cell attaches to a surface. The cell then grows and divides, forming microcolonies. Cells then secrete Vibrio exopolysaccharide (VPS) and matrix proteins that facilitate cell-cell and cell-surface attachment (1). Various mechanisms *regulat*e biofilms in *V. cholerae*, including two-component signal transduction systems (TCSs). The *V. cholerae* genome encodes 43 sensor histidine kinases (HKs) and 49 response regulators (RRs)(8, 39). The high number of HKs and RRs enables *V. cholerae to* regulate diverse cellular processes. Researchers systematically identified TCSs involved in biofilm regulation by measuring *vpsL* transcription to identify positive and negative biofilm regulators. One single-RR deletion, *carR* (VC1320), showed a significant increase in *vpsL* expression and is a negative regulator of biofilm formation (8).

The calcium-regulated response regulator *carR* and sensor histidine kinase *carS* (VC1319) are in a two-gene operon TCS whose transcription is downregulated in the presence of calcium, an environmental signal sensed by *V. cholerae* during the transition from fresh to seawater (14). Deletion of *carR* and *carS* increases biofilm biomass, as measured by biofilm volume, compared to wild type, whereas overexpression of either CarR or CarS decreases biofilm volume (13, 14). Indicating that CarR and CarS could be involved in biofilm dispersal. Biofilm dispersal occurs when cells begin to detach from the biofilm (14). The CarRS TCS is also essential for polymyxin B resistance, a cationic antimicrobial peptide.

As a canonical TCS, CarRS is predicted to use a phosphorelay-based signaling mechanism. However, it is unknown whether phosphorylation is important for CarR/S TCS function, or how CarRS affects biofilm formation, including when and where CarRS is expressed during biofilm formation. CarRS TCSs are important for AP sensing; thus far, the connection

between CarRS AP sensing and its effect on biofilm formation has not been shown and remains to be determined, which will help identify the role of CarRS phosphorylation and CAMP sensing in biofilm formation (14, 40). These key aspects are important for fitness in infection with *V. cholerae*.

3.2 **Results**

3.2.1. Identification of residues for phosphotransfer of CarS and CarR

Signals that activate the two-component regulatory system CarRS remain unknown, but the system is activated when cells are exposed to polymyxin B and defensin 5 (HD-5) (8). When a signal is detected, the sensor histidine kinase CarS is predicted to autophosphorylate and transfer the phosphoryl group to the response regulator CarR, thereby activating transcription of downstream target genes (32,33).

CarS is a sensor histidine kinase. Using the amino acid sequence, we identified residues important for phosphorylation: residues 222, 223, and 226 are predicted to be critical for kinase activity, phosphate activity, and dephosphorylation, respectively. We mutated residues H222, D223, and T226 to alanine (Figure 3.1A). H222A results in a residue that cannot be phosphorylated, D223A in a mutant unable to perform kinase activity, and T226A in an inability to dephosphorylate the cognate response regulator (7). We also identified residues important for phosphorylation, including a conserved aspartate residue 55 (Figure 3.1B). We mutated aspartate 55 to alanine or glutamate to generate phosphomimetic versions. D55A resulted in a CarR-inactive version, and D55E resulted in a CarR-active version.

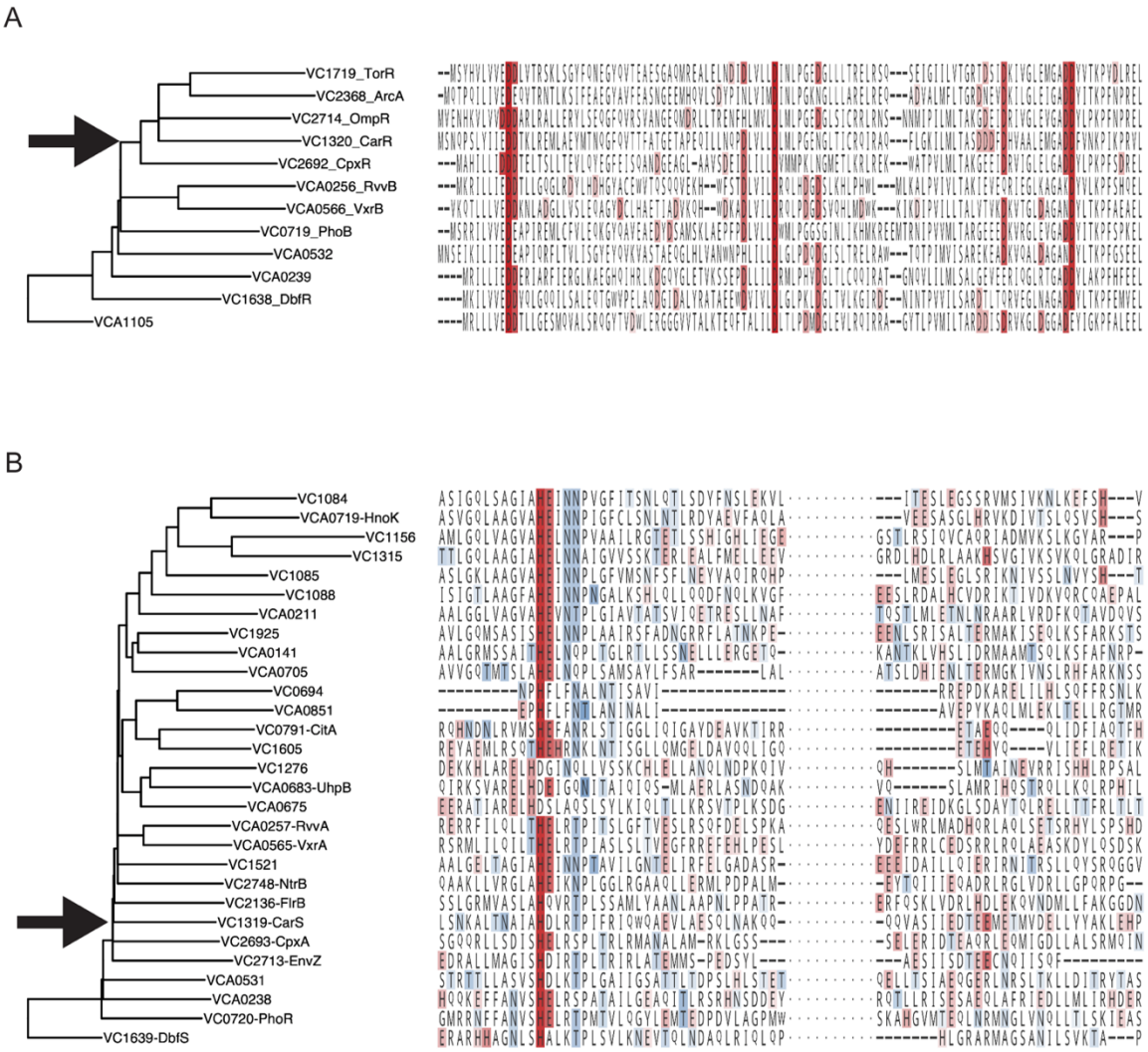

Figure 3.1 Identification of residues for phosphotransfer of CarS and CarR.

ClustalO amino acid sequence (right) and phylogenetic tree (left) of the A) Rec domain on OmpR-like response regulators and B) HiskA DHp domain-type sensor histidine kinases in *V. cholerae*. Phylogenetic trees were generated from sequence alignment by neighbor-joining using BLOSUM63.

3.2.2. CarRS Phosphorylation is important for cationic antimicrobial peptide resistance

Polymyxin B sensitivity of the phosphomimetic CarRS mutants was determined. Amino acid sequence and phylogenetic tree identified aspartate residue 55 as an important phosphorylation site in the REC domain of CarR (Figure 3.1A) and residues 222, 223, and 226 in CarS (Figure 3.1B). Mutations in CarR and in CarS had distinct effects on polymyxin B resistance. Mutations in the conserved phosphorylation site of CarR (*carR*^{D55A} and *carR*^{D55E}) reduced resistance to levels like the Δ*carR* mutant, with MIC values of 5.0–5.7 μg/ml (Figure 3.2 A). Δ*carS*, *carS*^{H222A}, and *carS*^{D223A} were highly sensitive (MIC = 1.3 μg/ml), whereas *carS*^{T226A} exhibited increased resistance (MIC = 64 μg/ml) compared with the wild type (MIC = 43 μg/ml) (Figure 3.2B). In the in vitro competitive index assay, *carR*^{D55A}, *carR*^{D55E}, *carS*^{H222A}, and *carS*^{D223A} were outcompeted by the wild type, while *carS*^{T226A} outcompeted the wild type after 24 hours of competition in the presence of polymyxin B (Figure 3.2C). These results indicate that phosphorylation of CarR and CarS is required for full polymyxin B resistance.

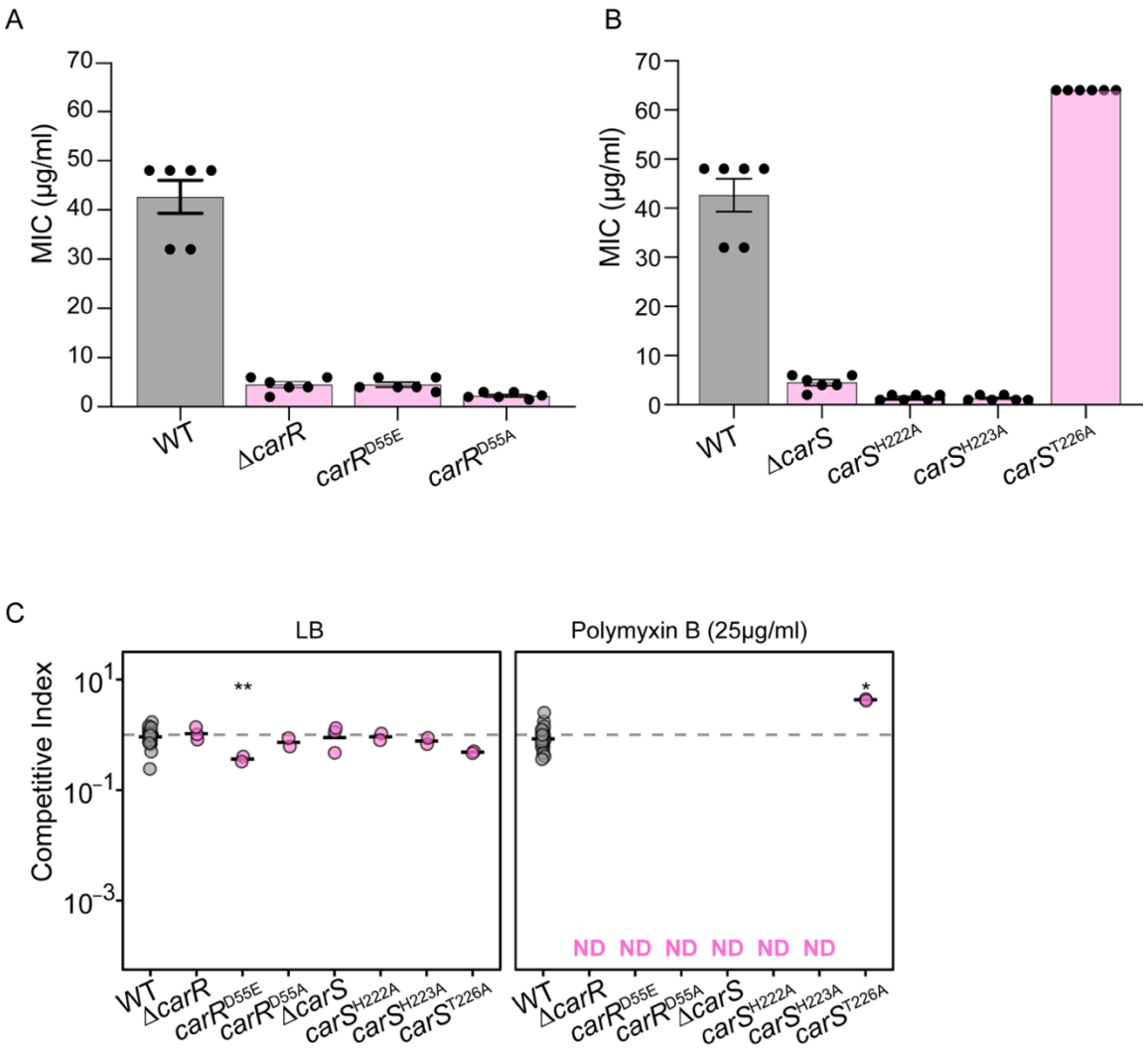

Figure 3.2 CarRS phosphorylation is important for polymyxin B resistance

A) Bar graph of polymyxin B resistance quantification of MIC for Δ*carS*, *carS*^{H222A}, *carS*^{D223A,} and *carS*^{T226A} mutants. B) Polymyxin B resistance quantification of MIC for Δ*carR*, *carR*^{D55A}, and *carR*^{D55E} mutants. Statistical analysis: n=2 biological replicates, one-way ANOVA and Dunnett's multiple comparisons test. Means from 3 individual biological replicates were compared to WT, and differences with an adjusted *P* value of < 0.01 were deemed significant; ** <0.01, *** <0.001, **** <0.0001. C) Scatter plot of relative fitness measured by in vitro competition of deletion mutants against the WT strain competed for 24hours. Competitive index (CI) values are plotted on a log10 scale. Means from ≥ 2 independent biological replicates were compared to WT by one-way ANOVA followed by Dunnett's multiple comparison test. Statistical comparisons were performed on log10(CI) values. Mean differences with an adjusted *P* value of ≤ 0.01 were deemed significant. *, $P \leq 0.01$; **, $P \leq 0.001$; ***, $P \leq 0.0001$; ns, not significant. Strains for which no colonies were recovered at the detection limit are indicated as ND (not detected) and were excluded from statistical comparisons.

3.2.3. Phosphorylation of CarRS affects expression of biofilm genes

Because CarRS negatively regulates biofilm formation, we measured promoter activity of the vps-II operon genes under standard laboratory conditions as a proxy for biofilm gene transcription (4). Transcriptional activity of the P*vpsL*-lux reporter was measured in the wild type and in the CarR and CarS mutants (Figure 3.3). The *carR*^{D55A}, Δ*carS*, *carS*^{H222A}, and *carS*^{D223A} mutants resulted in increased *vpsL* transcription; *carR*^{D55E} resulted in *vpsL* transcription like that of the wild type; and *carS*^{T226A} resulted in decreased *vpsL* transcription (Figure 3.3B). This indicates that CarR and CarS phosphorylation affects biofilm gene expression.

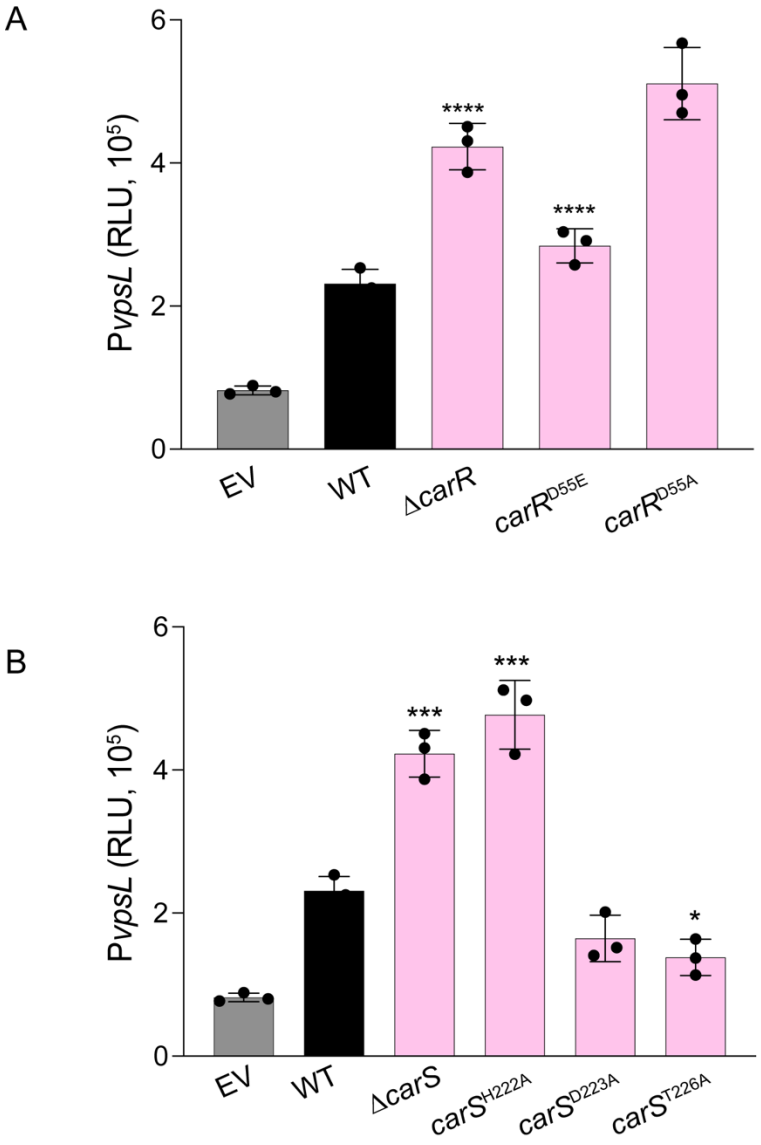

Figure 3.3 CarRS phosphorylation is important for biofilm gene expression.

Promoter activity of the transcription fusion P*vpsL-lux* was measured from cells grown to exponential phase in strains harboring either deletions or mutated versions of CarR or CarS. Bar graph of relative luminescent units (RLU) for A) Δ*carR*, *carR*^{D55A} and *carR*^{D55E} mutants; B) Δ*carS*, *carS*^{H222A}, *carS*^{D223A} and *carS*^{T226A} mutants. Statistical analysis: n=3 biological replicates, one-way ANOVA, and Dunnett's multiple comparisons test. Means from individual biological replicates of 3 were compared to WT, and differences with an adjusted *P* value of < 0.01 were significant; ** <0.01, *** <0.001, **** <0.0001.

3.2.4. CarRS phosphorylation and biofilm formation

Because CarRS negatively regulates biofilm formation and *vspL* expression, we examined how phosphomimetic mutants contribute to biofilm formation. Biofilm formation was quantified as biofilm volume (μm³). The Δ*carR* and *carR*^{D55A} strains tend to increase biofilm volume, while *carR*^{D55E} tends to show an intermediate biofilm volume between the Δ*carR* and wild-type strains (Figure 3.4A). The CarS mutants: Δ*carS, carS*^{H222A}, *carS*^{D223A}, and *carS*^{T226A} tend to show more biofilm volume compared to wild type (Figure 3.4B).

Figure 3.4 CarRS mutants and biofilm formation

Representative images of a flow cell biofilm experiment of WT and CarRS mutants. A) Δ*carR,* *carR*^{D55E}, and *carR*^{D55A} in LB. B) Δ*carS* and *carS*^{H222A}, *carS*^{D223A,} and *carS*^{T226A} mutants. Images of the biofilm were obtained at 40X magnification and generated using Imaris software; they are representative of ≥1 independent analysis. Scale bars = 15 μm. C) Bar graph of biofilm biomass as biofilm volume measured in (μm^3) using BiofilmQ. Graphs show the mean, with error bars representing the standard deviation. Statistical analysis: n=3 biological replicates per strain A) and n=2 biological replicates per strain (B).

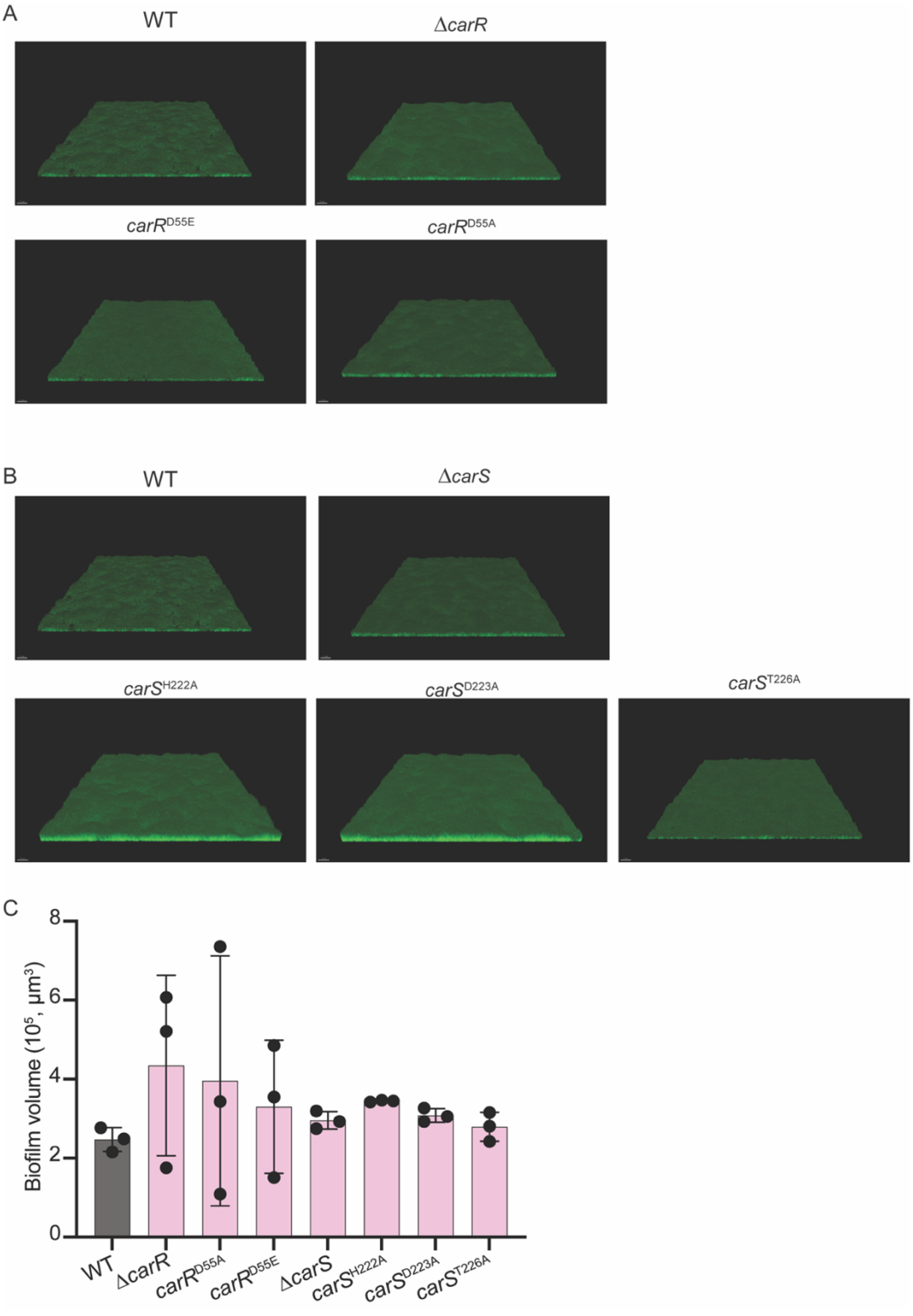
A
WT
ΔcarR
carRD55E
carRD55A
B
WT
ΔcarS
carSH222A
carSD223A
carST226A
C
Biofilm volume (10^5, μm^3)
0
2
4
6
8
WT
ΔcarR
carRD55A
carRD55E
ΔcarS
carSH222A
carSD223A
carST226A

3.2.5. CarR expression occurs during biofilm formation

To determine when and where in the biofilm *carR* is expressed, we used a fluorescent reporter in which the *carR* upstream regulatory region drives sfGFP expression with a constitutively transcribed mCardinal (41). *carR* expression was determined in wild-type and Δ*carR* strains grown under static biofilm conditions. We found that *carR* promoter activity is highest toward the top of the biofilm (Figure 3.5).

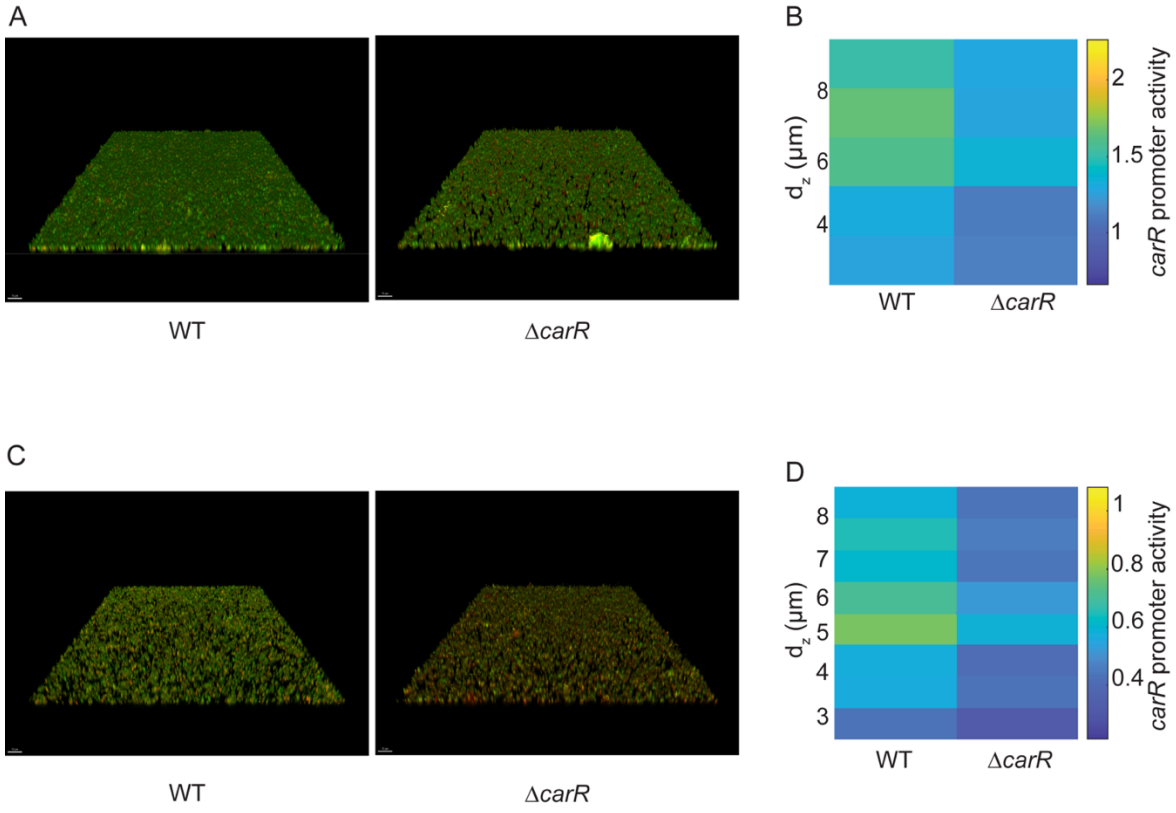

Figure 3.5 CarR is expressed during biofilm formation

Representative images of the static biofilm of WT and ΔcarR mutant with P*carR*-sfGFP expression. Images were obtained at 40X magnification of biofilm formation at 10 hours (A) and 24 hours (B). Images were generated in Imaris and represent 2 independent analyses. Scale bars = 10 μm. Kymographs of *carR* promoter activity based on P*carR*-sfGFP expression in WT and Δ*carR* during biofilm formation at 10 hours (C) and 24 hours (D). Biofilm depth is reported in μm, and relative *carR* expression is reported as a ratio of sfGFP intensity/mCardinal intensity.

Table 3.1 Bacterial strains and plasmids used in this work

Strain or plasmid	Description	Source
E. coli		
DH5α-λ*pir*	end*A1 hsdR17 gln*V44 (-supE44) thi-1 *recA gyrA*96 *rel*A1 φ80*dlac*Δ*(lacZ)M15* Δ*(lacZYA-argF)U169 zdg-232::Tn10 uidA::pir+*	47
S17-1λ*pir*	Tp^r Sm^r *rec Athi pro* r_k- m_{k+} RP4::2-Tc::MuKm Tn7 λ*pir*	48
V. cholerae		
FY_Vc_1	*Vibrio cholerae* O1 El Tor A1552, wild type, Rif^r	49
FY_Vc_628	Δ*lacZ,* Rif^r	50
FY_Vc_237	FY_Vc_1 Tn7*::gfp* Rif^r, Gm^r	51
FY_Vc_3274	Δ*carS* (VC1319), Rif^r	13
FY_Vc_3275	Δ*carS* (VC1319) Tn7*::gfp* Rif^r	13
FY_Vc_3282	Δ*carR* (VC1320), Rif^r	13
FY_Vc_3283	Δ*carR* (VC1320) Tn7*::gfp* Rif^r	13
FY_Vc_20788	*carR*^{D55E}, Rif^r	This study
FY_Vc_20789	*carR*^{D55A},Rif^r	This study
FY_Vc_20790	*carS*^{H222A},Rif^r	This study
FY_Vc_20791	*carS*^{D223A},Rif^r	This study
FY_Vc_20792	*carS*^{T226A}, Rif^r	This study
FY_Vc_4091	Δ*almG* (VC1576), Rif^r	8
FY_Vc_4094	Δ*almF* (VC1577), Rif^r	8
FY_Vc_4097	Δ*almE* (VC1578), Rif^r	8
FY_Vc_5653	Δ*CarR* + pBBR*lux vpsL* promoter, Rif^r Cm^r	
FY_Vc_20846	*carR*^{D55E}+ pBBR*lux vpsL* promoter, Rif^r Cm^r	This study

Strain or plasmid	Description	Source
FY_Vc_20847	*carR*^{D55A}+ pBBR*lux vpsL* promoter, Rif^r Cm^r	This study
FY_Vc_20848	Δ*carS* + pBBR*lux vpsL* promoter, Rif^r Cm^r	This study
FY_Vc_20849	*carS*^{H222A} + pBBR*lux vpsL* promoter, Rif^r Cm^r	This study
FY_Vc_20850	*carS*^{D223A} + pBBR*lux vpsL* promoter, Rif^r Cm^r	This study
FY_Vc_20851	*carS*^{T226A} + pBBR*lux vpsL* promoter, Rif^r Cm^r	This study
FY_Vc_20852	*carR*^{D55E}+ pBBRlux-vector	This study
FY_Vc_20853	*carR*^{D55A}+ pBBRlux-vector	This study
FY_Vc_20854	Δc*arS*+ pBBRlux-vector	This study
FY_Vc_20855	*carS*^{H222A}+ pBBRlux-vector	This study
FY_Vc_20856	*carS*^{D223A}+ pBBRlux-vector	This study
FY_Vc_20857	*carS*^{T226A}+ pBBRlux-vector	This study
Plasmids		
pFY_23	pGP704 derivative; mob-ori, sacB, Amp^r	G. Schoolnik
pFY_117	pGP704::mTn7-*gfp*, Gm^r, Amp^r	52
pFY_118	oriR6K helper plasmid, *mob-oriT,* provides the Tn7 transposition function in *trans,* Amp^r	52
pFY_8386	pGP704sacB-*carR*^{D55A}	This study
pFY_8394	pGP704sacB-*carR*^{D55E}	This study
pFY_8396	pGP704sacB-*carS*^{H222A}	This study
pFY_8388	pGP704sacB-*carS*^{D223A}	This study
pFY_8387	pGP704sacB-*carS*^{T226A}	This study
pFY_8397	pGP704sacB-*carRS* (VC1319-20)	This study

Strain or plasmid	Description	Source
pFY_8398	pGP704sacB-*dbfRS* (VC1638-39)	This study
pFY_691	*luxCDABE*-based promoter fusion vector, Cm^r	52
pFY_3406	pBBR*lux vpsL* promoter, Cm^r (-607, +158)	54

3.3 **Discussion**

Our findings show that CarRS phosphorylation states partially influence phenotypic outcomes, affecting both antimicrobial resistance and biofilm formation. Mutants defective in CarS phosphorylation and kinase activity decrease polymyxin B resistance and showed a trend toward increased biofilm formation. The CarS-phosphatase mutant increases polymyxin B resistance. CarR mutations in the conserved aspartate residue for phosphorylation decreased polymyxin B resistance and showed a trend toward increased biofilm formation compared to wild type. Finally, *carR* expression is detected during biofilm formation.

Signals sensed by CarRS TCSs during biofilm formation remain unidentified. Previous work has shown that calcium represses *carR* expression, which *V. cholerae* encounters in aquatic environments (14), and that *carR* is critical for polymyxin B resistance (40). This work shows that CarRS activation contributes to antimicrobial peptide resistance. Mutations affecting CarS function showed that these mutations are important for sensor histidine kinase activity. The CarR phosphorylation-site mutants did not result in constitutive on- and off-states of the response regulator.

I observed that *carR* expression occurs during biofilm formation in wild-type cells, although further studies are needed to determine when and where *carR* expression occurs. These initial studies were done in statically grown biofilms, which results in a confined biofilm where quorum sensing (42, 43) negatively regulates biofilm formation; further testing under different

biofilm-forming conditions is needed. Furthermore, Δ*carR* exhibits increased *vpsL* expression under planktonic growth conditions. The impact of CarRS phosphorylation under biofilm-grown conditions needs to be explored.

These data provide insights into the CarRS TCS system, revealing its dual role in mediating antimicrobial resistance and regulating biofilm formation in *V. cholerae*

3.4 **Material and Methods**

3.4.1. Bacterial strains, plasmids, and growth conditions

Table 1 lists the strains and plasmids used in this study. All *V. cholerae* and *E. coli* strains were grown in Luria-Bertani (LB) medium (0.5% yeast extract, 1% tryptone, 1% NaCl, pH 7.5) at 30˚C and 37˚C, respectively, with 200 rpm shaking, unless otherwise indicated. LB agar medium included granulated agar (BD Difco, Franklin Lakes, NJ) at 1.5% (wt/vol). Antibiotics and inducers were used, when necessary, at the following concentrations: ampicillin 100 μg/mL and rifampin 100 μg/mL. Unless otherwise specified, overnight cultures were prepared as follows: strains were streaked from frozen glycerol stock onto an LB-agar plate and grown at 30˚C overnight. 5 colonies were then inoculated into 5 mL of LB medium and grown overnight at 30˚C with aeration (200 rpm).

3.4.2. Strain and plasmid construction

Plasmids were constructed using standard cloning methods for the Gibson Assembly recombinant DNA technique (New England Biolabs, Ipswich, MA). Restriction enzymes were purchased from New England Biolabs. Gene-in-frame deletions were performed using an allelic exchange of the native open reading frame (ORF) with the truncated ORF as previously described (44). Polymerase chain reactions (PCRs) were carried out with primers purchased from Integrated DNA Technologies, and plasmid constructs were performed at Genewiz/Azenta Life Sciences (Chelmsford, MA). For chromosomal point mutant constructs,

the native gene, plus ~ 500 base pairs (bp) upstream and downstream, was cloned into the suicide plasmid pGP704*sacB*28. This construct was mutagenized using the Q5 mutagenesis kit (New England BioLabs) to introduce point mutations. Gene replacements were performed by allelic exchange in the deletion-background strain, as previously described (44). All *V. cholerae* sequences were amplified from genomic DNA isolated from the *V. cholerae* A1552 strain. The resulting plasmid was transformed into *E. coli* and DH5α-λ*pir* donor strain and introduced into the *V. cholerae* A1552 strain by conjugation.

3.4.3. Minimum inhibitory concentration

V. cholerae liquid cultures grown overnight at 30˚C with 200 rpm shaking were diluted to OD_{600} 0.3, and 150µL were spread on 15 mL 150 × 15 mm LB agar medium plates, dried, and an E-strip of polymyxin B (Thermo Fisher).

3.4.4. Biofilm imaging and image analysis

V. cholerae strains tagged with GFP were streaked on LB plates and incubated at 30˚C overnight. 5 single colonies from the overnight-grown plates were inoculated into 5 mL LB grown overnight at 30˚C with 200 rpm shaking. Normalized to an OD_{600} of 0.015, cells were then injected into a µ-Slide VI 0.4 uncoated (Ibidi, Martinsried, Germany). After injection, cells were allowed to attach to the flow cell surface for 1 hour at 30˚C. Flow of 2% v/v LB was initiated at 7.5 ml/hour and continued for 24 hours. Biofilms were imaged using Confocal laser scanning microscopy (CLSM). Images of the biofilm were captured with an LSM 880 (Zeiss, Jena, Germany), using an excitation wavelength of 488 nm and an emission of 543 nm. Three-dimensional(3D) images of the biofilm were processed using Imaris software (Bitplane, Zurich, Switzerland). All image processing parameters in Imaris (opacity, min/max, etc.) were kept identical across all image sets for accurate comparison. Quantitative analysis was done using BiofilmQ software.

Bibliography

1. Teschler JK, Zamorano-Sánchez D, Utada AS, Warner CJA, Wong GCL, Linington RG, Yildiz FH. 2015. Living in the matrix: assembly and control of Vibrio cholerae biofilms. Nat Rev Microbiol 13:255–268.

2. Zhou Y, Lee ZL, Zhu J. 2020. On or Off: Life-Changing Decisions Made by Vibrio cholerae Under Stress. Infect Microbes Dis 2:127–135.

3. Krell T, Lacal J, Busch A, Silva-Jiménez H, Guazzaroni M-E, Ramos JL. 2010. Bacterial sensor kinases: diversity in the recognition of environmental signals. Annu Rev Microbiol 64:539–559.

4. Gao R, Stock AM. 2009. Biological insights from structures of two-component proteins. Annu Rev Microbiol 63:133–154.

5. Willett JW, Kirby JR. 2012. Genetic and biochemical dissection of a HisKA domain identifies residues required exclusively for kinase and phosphatase activities. PLoS Genet 8:e1003084.

6. Huynh TN, Stewart V. 2011. Negative control in two-component signal transduction by transmitter phosphatase activity. Mol Microbiol 82:275–286.

7. Huynh TN, Noriega CE, Stewart V. 2010. Conserved mechanism for sensor phosphatase control of two-component signaling revealed in the nitrate sensor NarX. Proc Natl Acad Sci U S A 107:21140–21145.

8. Teschler JK, Cheng AT, Yildiz FH. 2017. The Two-Component Signal Transduction System VxrAB Positively Regulates Vibrio cholerae Biofilm Formation. J Bacteriol 199:e00139-17, e00139-17.

9. Floyd KA, Lee CK, Xian W, Nametalla M, Valentine A, Crair B, Zhu S, Hughes HQ, Chlebek JL, Wu DC, Hwan Park J, Farhat AM, Lomba CJ, Ellison CK, Brun YV, Campos-Gomez J, Dalia AB, Liu J, Biais N, Wong GCL, Yildiz FH. 2020. c-di-GMP modulates type IV MSHA pilus retraction and surface attachment in Vibrio cholerae. Nat Commun 11:1549.

10. Jones CJ, Utada A, Davis KR, Thongsomboon W, Zamorano Sanchez D, Banakar V, Cegelski L, Wong GCL, Yildiz FH. 2015. C-di-GMP Regulates Motile to Sessile Transition by Modulating MshA Pili Biogenesis and Near-Surface Motility Behavior in Vibrio cholerae. PLOS Pathog 11:e1005068.

11. Yildiz FH, Schoolnik GK. 1999. *Vibrio cholerae* O1 El Tor: Identification of a gene cluster required for the rugose colony type, exopolysaccharide production, chlorine resistance, and biofilm formation. Proc Natl Acad Sci 96:4028–4033.

12. Berk V, Fong JCN, Dempsey GT, Develioglu ON, Zhuang X, Liphardt J, Yildiz FH, Chu S. 2012. Molecular architecture and assembly principles of Vibrio cholerae biofilms. Science 337:236–239.

13. Teschler JK, Nadell CD, Drescher K, Yildiz FH. 2022. Mechanisms Underlying Vibrio cholerae Biofilm Formation and Dispersion. Annu Rev Microbiol 76:503–532.

14. Identification of a calcium-controlled negative regulatory system affecting Vibrio cholerae biofilm formation.

15. Clemens JD, Nair GB, Ahmed T, Qadri F, Holmgren J. 2017. Cholera. Lancet 390:1539–1549.

16. Matson JS, Yoo HJ, Hakansson K, DiRita VJ. 2010. Polymyxin B Resistance in El Tor *Vibrio cholerae* Requires Lipid Acylation Catalyzed by MsbB. J Bacteriol 192:2044–2052.

17. Liu Y, Xu T, Wang Q, Huang J, Zhu Y, Liu X, Liu R, Yang B, Zhou K. 2022. Vibrio cholerae senses human enteric α-defensin 5 through a CarSR two-component system to promote bacterial pathogenicity. Commun Biol 5:559.

18. Mathieu-Denoncourt A, Whitfield GB, Vincent AT, Berne C, Pauzé-Foixet J, Mahieddine FC, Brun YV, Duperthuy M. 2025. The carRS-ompV-virK operon of Vibrio cholerae senses antimicrobial peptides and activates the expression of multiple resistance systems. Sci Rep 15:13686.

19. Purcell AB, Voss BJ, Trent MS. 2022. Diacylglycerol Kinase A Is Essential for Polymyxin Resistance Provided by EptA, MCR-1, and Other Lipid A Phosphoethanolamine Transferases. J Bacteriol 204:e00498-21.

20. Harper M, Wright A, St. Michael F, Li J, Deveson Lucas D, Ford M, Adler B, Cox AD, Boyce JD. 2017. Characterization of Two Novel Lipopolysaccharide Phosphoethanolamine Transferases in Pasteurella multocida and Their Role in Resistance to Cathelicidin-2. Infect Immun 85:e00557-17.

21. Malinverni JC, Silhavy TJ. 2009. An ABC transport system that maintains lipid asymmetry in the Gram-negative outer membrane. Proc Natl Acad Sci 106:8009–8014.

22. Nakayama T, Zhang-Akiyama Q-M. 2017. *pqiABC* and *yebST* , Putative *mce* Operons of Escherichia coli, Encode Transport Pathways and Contribute to Membrane Integrity. J Bacteriol 199.

23. Mathur J, Waldor MK. 2004. The *Vibrio cholerae* ToxR-Regulated Porin OmpU Confers Resistance to Antimicrobial Peptides. Infect Immun 72:3577–3583.

24. Chatterjee A, Dutta PK, Chowdhury R. 2007. Effect of fatty acids and cholesterol present in bile on expression of virulence factors and motility of Vibrio cholerae. Infect Immun 75:1946–1953.

25. Fleurie A, Zoued A, Alvarez L, Hines KM, Cava F, Xu L, Davis BM, Waldor MK. 2019. A Vibrio cholerae BolA-Like Protein Is Required for Proper Cell Shape and Cell Envelope Integrity. mBio 10:e00790-19.

26. Turner J, Cho Y, Dinh N-N, Waring AJ, Lehrer RI. 1998. Activities of LL-37, a Cathelin-Associated Antimicrobial Peptide of Human Neutrophils. Antimicrob Agents Chemother 42:2206–2214.

27. Keshri AK, Rawat SS, Chaudhary A, Sharma S, Kapoor A, Mehra P, Kaur R, Mishra A, Prasad A. 2025. LL-37, the master antimicrobial peptide, its multifaceted role from combating infections to cancer immunity. Int J Antimicrob Agents 65:107398.

28. Nesper J, Lauriano CM, Klose KE, Kapfhammer D, Kraiß A, Reidl J. 2001. Characterization of *Vibrio cholerae* O1 El Tor *galU* and *galE* Mutants: Influence on Lipopolysaccharide Structure, Colonization, and Biofilm Formation. Infect Immun 69:435–445.

29. Henderson JC, Fage CD, Cannon JR, Brodbelt JS, Keatinge-Clay AT, Trent MS. 2014. Antimicrobial Peptide Resistance of *Vibrio cholerae* Results from an LPS Modification Pathway Related to Nonribosomal Peptide Synthetases. ACS Chem Biol 9:2382–2392.

30. Sposato D, Pederzoli C, Bufano M, Sciò P, Rossi L, Leoni L, Rampioni G, Visca P, Coluccia A, Imperi F. 2025. Structure-function relationship of the Pseudomonas aeruginosa AsmA-like proteins YhdP and YdbH involved in outer membrane biogenesis. Protein Sci Publ Protein Soc 34:e70227.

31. Ruiz N, Davis RM, Kumar S. 2021. YhdP, TamB, and YdbH Are Redundant but Essential for Growth and Lipid Homeostasis of the Gram-Negative Outer Membrane. mBio 12:e02714-21.

32. Knowles TJ, Scott-Tucker A, Overduin M, Henderson IR. 2009. Membrane protein architects: the role of the BAM complex in outer membrane protein assembly. Nat Rev Microbiol 7:206–214.

33. Kim KH, Aulakh S, Paetzel M. 2012. The bacterial outer membrane β-barrel assembly machinery. Protein Sci 21:751–768.

34. Kim KH, Paetzel M. 2011. Crystal Structure of Escherichia coli BamB, a Lipoprotein Component of the β-Barrel Assembly Machinery Complex. J Mol Biol 406:667–678.

35. Webb CT, Selkrig J, Perry AJ, Noinaj N, Buchanan SK, Lithgow T. 2012. Dynamic association of BAM complex modules includes surface exposure of the lipoprotein BamC. J Mol Biol 422:545–555.

36. Ko D, Sung D, Kim TY, Choi G, Bang Y-J, Choi SH. 2023. CarRS Two-Component System Essential for Polymyxin B Resistance of Vibrio vulnificus Responds to Multiple Host Environmental Signals. Microbiol Spectr 11:e00305-23.

37. Thai VC, Stubbs KA, Sarkar-Tyson M, Kahler CM. 2023. Phosphoethanolamine Transferases as Drug Discovery Targets for Therapeutic Treatment of Multi-Drug Resistant Pathogenic Gram-Negative Bacteria. Antibiotics 12:1382.

38. Ridyard KE, Elsawy M, Mattrasingh D, Klein D, Strehmel J, Beaulieu C, Wong A, Overhage J. 2023. Synergy between Human Peptide LL-37 and Polymyxin B against Planktonic and Biofilm Cells of Escherichia coli and Pseudomonas aeruginosa. Antibiotics 12:389.

39. Kitts G, Rogers A, Teschler JK, Park JH, Trebino MA, Chaudry I, Erill I, Yildiz FH. 2023. The Rvv two-component regulatory system regulates biofilm formation and colonization in Vibrio cholerae. PLOS Pathog 19:e1011415.

40. Bilecen K, Fong JCN, Cheng A, Jones CJ, Zamorano-Sánchez D, Yildiz FH. 2015. Polymyxin B Resistance and Biofilm Formation in Vibrio cholerae Are Controlled by the Response Regulator CarR. Infect Immun 83:1199–1209.

41. Trebino MA, Kitts G, Haycocks JRJ, Wheat R, Chaudry I, Park JH, Erill I, Grainger DC, Yildiz FH. 2025. Parallel regulatory circuits orchestrate biofilm formation in response to c-di-GMP levels and growth phase. PLOS Genet 21:e1011870.

42. Hammer BK, Bassler BL. 2003. Quorum sensing controls biofilm formation in *Vibrio cholerae*. Mol Microbiol 50:101–104.

43. Bridges AA, Bassler BL. 2019. The intragenus and interspecies quorum-sensing autoinducers exert distinct control over Vibrio cholerae biofilm formation and dispersal. PLoS Biol 17:e3000429.

44. Fong JCN, Karplus K, Schoolnik GK, Yildiz FH. 2006. Identification and Characterization of RbmA, a Novel Protein Required for the Development of Rugose Colony Morphology and Biofilm Structure in *Vibrio cholerae*. J Bacteriol 188:1049–1059.